University of Alabama in Huntsville
LOUIS

Theses | UAH Electronic Theses and Dissertations

2014

Three-dimensional modeling of an ideal nozzle for advanced propulsion

Kevin Schillo

Follow this and additional works at: https://louis.uah.edu/uah-theses

Recommended Citation
Schillo, Kevin, "Three-dimensional modeling of an ideal nozzle for advanced propulsion" (2014). *Theses*. 92.
https://louis.uah.edu/uah-theses/92

This Thesis is brought to you for free and open access by the UAH Electronic Theses and Dissertations at LOUIS. It has been accepted for inclusion in Theses by an authorized administrator of LOUIS.

THREE-DIMENSIONAL MODELING OF AN IDEAL NOZZLE FOR ADVANCED PROPULSION

by

KEVIN SCHILLO

A THESIS

Submitted in partial fulfillment of the requirements
for the degree of Master of Science in Aerospace Systems Engineering
in
The Department of Mechanical and Aerospace Engineering
of
The School of Graduate Studies
of
The University of Alabama in Huntsville

HUNTSVILLE, ALABAMA

2014

In presenting this thesis in partial fulfillment of the requirements for a master's degree from The University of Alabama in Huntsville, I agree that the Library of this University shall make it freely available for inspection. I further agree that permission for extensive copying for scholarly purposes may be granted by my advisor or, in his/her absence, by the Chair of the Department or the Dean of the School of Graduate Studies. It is also understood that due recognition shall be given to me and to The University of Alabama in Huntsville in any scholarly use which may be made of any material in this thesis.

(student signature) (date) 4/7/14

THESIS APPROVAL FORM

Submitted by Kevin Schillo in partial fulfillment of the requirements for the degree of Master of Science in Aerospace Systems Engineering and accepted on behalf of the Faculty of the School of Graduate Studies by the thesis committee.

We, the undersigned members of the Graduate Faculty of the University of Alabama in Huntsville, certify that we have advised and/or supervised the candidate on the work described in this thesis. We further certify that we have reviewed the thesis manuscript and approve it in partial fulfillment of the requirements of the degree of Master of Science in Aerospace Systems Engineering.

4/7/14 Committee Chair
Dr. Jason T. Cassibry (Date)

4/7/14
Dr. Robert A. Frederick

4/7/14
Dr. Kunning G. Xu

Department Chair
Dr. Keith Hollingsworth

College Dean
Dr. Shankar Mahalingam

Graduate Dean
Dr. David Berkowitz

ABSTRACT
The School of Graduate Studies
The University of Alabama in Huntsville

Degree_____Master of Science_____College/Dept.__Engineering/Mechanical and Aerospace Engineering_____

Name of Candidate_____Kevin Schillo_____
Title__Three-Dimensional Modeling of an Ideal Nozzle for Advanced Propulsion
_____

Advanced propulsion systems such as pulsed fission and fusion rockets hold the potential for opening up the solar system in ways few other propulsion technologies can. The University of Alabama in Huntsville is exploring one such concept in the form of pulsed z-pinch fusion propulsion. One of the technical hurdles to utilizing any pulsed fusion concept is the conversion from an isotropic expansion of a plasma into directed motion to produce thrust. This thesis investigates three dimensional modeling of pulsed nozzle performance in which the initial gas is a cylindrical gas column, emulating the initial conditions found in pulsed plasma discharges common in fusion experiments. Two nozzle geometries were investigated, a pusher plate and a hemispherical nozzle.

Simulations of these systems were conducted using SPFMax, a recently developed smoothed particle hydrodynamics code (SPH). The SPH method was chosen because it is naturally adaptive and accurate for resolving the vacuum/gas boundary which always exists in pulsed fusion systems. Argon plasma was used to compare the two systems to determine which offers better performance. The plasma was also subjected to a wide variety of shapes and initial conditions to determine what would offer higher performance for the two systems.

Abstract Approval: Committee Chair _____

Department Chair _____

Graduate Dean _____

ACKNOWLEDGEMENTS

I would first like to thank my advisor Dr. Jason Cassibry for his tireless efforts in helping me throughout my time working on this research. Every time that I struggled to figure something out, he would not hesitate to help me as much as humanely possible. I remain in awe of the brilliance, dedication, and passion he has for this field of study. Of all the research projects I have worked on throughout my studies and career thus far, I have felt greater passion for this than I have for anything else. I cannot thank him enough for everything that he has done for me.

This work was supported by a subcontract from NASA MSFC on grant NNM11AA01A as part of a NASA Innovative Advanced Concepts (NIAC) award. I will be forever grateful for having had this opportunity.

The Propulsion Research Center is an amazing facility, and I am very thankful for all of the staff that helps to make it such a wonderful work environment.

I would also like to thank my roommate Tyler Maddox for tolerating me throughout our time together in graduate school.

I am deeply indebted to all the members of my family who have provided me with nothing but unceasing love and support throughout my entire life. In all of my great triumphs and crushing failures, you were always there for me. I'm very grateful for my sisters Mary, Katie, and Megan who have always managed to put up with me. I'm extremely appreciative of my brother Mark, who knows and understands me better than just about anyone. I would especially like to thank my parents, who always encouraged

me to pursue my dreams, and who were fully confident that I would finish my thesis in a timely manner.

TABLE OF CONTENTS

LIST OF FIGURES ..... **x**

LIST OF TABLES ..... **xii**

LIST OF SYMBOLS ..... **xiii**

Chapter

1 INTRODUCTION **1**

2 BACKGROUND **7**

2.1 Overview of Nuclear Propulsion Concepts 7

2.2 Overview of Magnetic Nozzle Concepts 18

2.2.1 Steady-State Magnetic Nozzles 19

2.2.2 Pulsed Magnetic Nozzles 22

2.3 Solid-State Pulsed Nozzles 25

3 SPFMax **27**

3.1 Introduction 27

3.2 Distmesh 28

3.3 Smoothed Particle Hydrodynamics 29

3.4 Euler Equations 32

3.5 Test Cases 32

3.5.1 Shock Tube 33

3.5.2 Verification Procedure 33

3.5.3 Expansion of a Gas Sphere 38

4 PROPULSION SIMULATIONS 43

4.1 Introduction 43

4.2 Nozzle Performance Results 46

4.3 Pusher Plate Performance Results 59

5 CONCLUSIONS 64

REFERENCES 68

LIST OF FIGURES

Figure Page

2.1 Mission requirements for different propulsion systems [6]. 8

2.2 Orion spacecraft [11]. 9

2.3 Orion pulse unit [12]. 10

2.4. Illustration of Collision of FRC Plasmoid with the Liner [27]. 17

2.5. VASIMR Engine [35]. 20

2.6. Steady-state fusion propulsion concept [37]. 21

2.7. Pulsed magnetic nozzle operation [6]. 22

2.8 VISTA magnetic thrust chamber operation [24]. 23

3.1 Comparison between SPFMax and analytical solution for temperature. 35

3.2 Comparison between SPFMax and analytical solution for density. 35

3.3 Comparison between SPFMax and analytical solution for pressure. 36

3.4 Log-log plot of temperature convergence. Slope is -0.69 37

3.5 Log-log plot of density convergence. Slope is -0.3 37

3.6 Log-log plot of pressure convergence. Slope is -0.58 38

3.7 Initial gas sphere. 39

3.8 Gas sphere at 10 microseconds. 40

3.9 Gas sphere at 20 microseconds. 40

3.10 Expansion velocity of gas sphere. 41

4.1 Cross-section of nozzle and propellant. 45

4.2 Nozzle geometry with r_{gn} of 0.05 and l_{gn} of 0.1. 47

4.3 Nozzle geometry with r_{gn} of 0.25 and l_{gn} of 1.0. 47

4.4 Nozzle with pancake-shaped propellant mass. 54

4.5 Nozzle specific impulse. 55

4.6 Nozzle propulsion efficiency. 55

4.7 Propellant ejection from nozzle at 0.84 microseconds. 56

4.8 Propellant ejection from nozzle at 1.5 microseconds. 57

4.9 Propellant ejection from nozzle at 4.7 microseconds. 58

4.10 Pancake-shaped propellant against the surface of the pusher plate. 59

4.11 Pusher plate specific impulse. 61

4.12 Pusher plate propulsion efficiency. 61

4.13 Ejection of propellant gas particles from pusher plate. 62

LIST OF TABLES

Table Page

4-1 Nozzle performance at 1 eV and 10^{24} number density. 48

4-2 Nozzle performance at 1 eV and 10^{26} number density. 49

4-3 Nozzle performance at 1 eV and 10^{28} number density. 49

4-4 Nozzle performance at 100 eV and 10^{24} number density. 50

4-5 Nozzle performance at 100 eV and 10^{26} number density. 50

4-6 Nozzle performance at 100 eV and 10^{28} number density. 51

4-7 Nozzle performance at 1,000 eV and 10^{24} number density. 51

4-8 Nozzle performance at 1,000 eV and 10^{26} number density. 52

4-9. Nozzle performance at 1,000 eV and 10^{28} number density. 52

4-10 Pusher plate performance with pancake-shaped propellant. 60

LIST OF SYMBOLS

SYMBOL	DEFINITION
A	Particle property
a	Acceleration
C	Convergence constant
C_v	Heat capacity at constant volume
dr'	Differential volume element
E	Energy
g_0	Gravitational acceleration at the Earth's surface
h	Radius of influence
I_{sp}	Specific impulse
$L1_\rho$	Density L1 norm
l_{gn}	Ratio of propellant gas length to gas radius
m_0	Initial mass
m_f	Final mass
m_p	Propellant mass
$\dot{m}$	Mass flow rate
p	Pressure
R_g	Propellant gas radius
R_n	Nozzle radius
r	Particle position
r_{gn}	Ratio of propellant gas radius to nozzle radius

T_0	Initial temperature
u_{max}	Maximum expansion velocity
v_e	Exhaust velocity
$\vec{V}$	Velocity vector
v_z	Propellant velocity in positive z direction
W	Smoothing kernel function
x_n	L1 error
ΔV	Change in velocity
η	Propulsion efficiency
κ	Smoothing function constant at a given location
ρ	Density

To my nephew Michael, I look forward to welcoming you into the world.

"There can be no thought of finishing, for aiming at the stars, both literally and figuratively, is the work of generations, but no matter how much progress one makes there is always the thrill of just beginning."

—Robert Hutchings Goddard

CHAPTER 1

INTRODUCTION

Since the dawn of spaceflight, humanity has dreamed of writing the next and arguably greatest chapter not only in the history of our civilization, but that of all life on Earth: the expansion of our biosphere beyond the peripheries of our home planet. But as with any great endeavor, great challenges must be overcome in order to turn this bold vision of the future into a reality.

While rocket propulsion has enabled mankind to break free from the confines of Earth, the physics that make this possible also impose great limits upon a rocket's performance capabilities. This is illustrated by the Tsiolkovsky rocket equation, which and can be expressed as:

$$\Delta V = I_{sp} g_0 \, ln \frac{m_o}{m_f} \tag{1.1}$$

This equation can be rearranged as:

$$\frac{m_f}{m_0} = e^{-\Delta V/(I_{sp} g_0)} \tag{1.2}$$

It is clear from this equation that an increase in the required ΔV of a spacecraft's mission leads to an exponential increase in the amount of propellant needed. It is also apparent from this equation that a higher specific impulse reduces the amount of propellant required for a given mission.

Chemical rockets are used as launch vehicles due to the high thrust levels that they offer. However, there is a fixed upper limit for the amount of energy that can be stored in the chemical bonds of propellants, and this in turn imposes a low value on the specific impulse that can be offered by a chemical rocket. This low specific impulse necessitates that chemical rockets use large amounts of propellant while offering comparatively small payload mass fractions. The practical use of chemical propulsion would be pushed to its limit by a manned Mars mission. Such an endeavor would require a very massive spacecraft, with the majority of the mass being propellant. The mission duration would also be very long, with most mission concepts lasting more than a year. In all likelihood, such a project would suffer the same fate that befell the Apollo program.

Electric propulsion systems are capable of delivering arbitrarily large amounts of energy to propellant, and as such offer specific impulses far beyond the capabilities of chemical systems. However, the power that they can deliver to propellant is limited by the mass of an onboard power source. An electric propulsion system capable of generating high thrust levels would be prohibitively massive if it were to use existing spacecraft power systems. This is the reason why current electric propulsion systems have very low thrust levels, which are orders of magnitude lower than thrust levels offered by chemical rockets [1]. Such systems are effective for satellite station-keeping and propelling small deep-space probes, but are not practical for manned missions.

The obvious solution to this problem is to utilize a propulsion system that offers both high thrust and high specific impulse. Systems with this capability include nuclear thermal, nuclear electric, and fusion rockets.

A nuclear thermal rocket operates by passing a propellant fluid through a nuclear reactor, which increases the enthalpy of the propellant before expanding it in a nozzle to generate thrust. Reactor fuels have energy densities on the order of 10^7 times greater than those offered by chemical propellants. This offers exhaust velocities far greater than that of chemical propulsion while also offering high thrust-to-weight ratios [2]. A disadvantage of this system is that many nuclear thermal rocket designs generate highly radioactive exhaust products. This makes the environmental impact from testing such a rocket a subject of serious concern. Political hurdles present an additional obstacle to any spacecraft system that utilizes nuclear power.

A nuclear electric rocket converts the thermal energy generated by an onboard nuclear reactor into electrical energy, which is then used to drive an electric propulsion system. This can generate thrust levels far greater than that of any existing electric propulsion system while also offering a specific impulse greater than that offered by nuclear thermal rockets. Unfortunately, the efficiency of nuclear electric systems is limited by the Carnot cycle, and consequently large amounts of waste heat are generated that must be rejected with large radiators, which contributes greatly to the mass of the spacecraft [3].

Fusion propulsion has several advantages over nuclear thermal and nuclear electric propulsion. The plasma exhaust from a fusion propulsion system can be converted directly into thrust, eliminating the need for an inefficient conversion between thermal and electric power. Because of this, fusion systems offer much higher specific power ratios and specific impulses than those offered by either nuclear thermal or nuclear electric rockets. This is what makes fusion especially attractive compared to other

propulsion systems. If fully developed, this technology could not only make a manned Mars mission possible, but also make it economical and routine in the long term.

Any project that culminates in the first manned mission to Mars cannot be allowed to suffer the same fate of the Apollo program, in which a major advancement in human spaceflight was followed by dramatically less ambitious programs that stifled rather than hastened mankind's expansion into the cosmos. It is for this reason that a fusion spacecraft cannot be allowed to be a single-use vehicle; it must be reusable, which will help drive down the costs of future missions and enable the construction of a thriving infrastructure beyond the confines of Earth.

Pulsed systems in particular are attractive because of the brief interaction time between the plasma and the surface of what it pushes against, often on the order of a few microseconds. This time is often too short for the heat from the plasma to cause extensive damage to the propulsion surface.

Many of the early research projects that investigated pulsed nuclear propulsion focused on detonating nuclear explosives behind a spacecraft to provide propulsion. A changing political climate forced the abandonment of concepts such as this, and that is unlikely to change in the near future. It must therefore be assumed that using conventional nuclear explosives for propulsion will always face seemingly insurmountable political opposition.

However, there are many pulsed fusion propulsion concepts that do not rely on conventional nuclear explosives. One ongoing effort is being conducted at the University of Alabama in Huntsville involves Z-pinch pulsed fusion. Before any experiments can be conducted, it is vital to create simulations of the experiments that can be done with

available equipment. This offers a more systematic approach to developing advanced propulsion concepts within budget constraints.

The need to create accurate simulations of plasmas for propulsion applications was part of the motivation behind the creation of SPFMax, a smoothed particle hydrodynamics code recently developed at the University of Alabama in Huntsville. This thesis investigates the utilization of SPFMax in the simulation of pulsed propulsion experiments that may be conducted in the future.

Due to the recent development of SPFMax, it was necessary to verify the code with relevant test cases to confirm that the physics is modeled accurately. To determine if this is the case, SPFMax was first used to simulate two problems with known solutions in order to assess the code's accuracy. The first was the capturing of shocks and rarefaction waves in the classic shock tube problem, and the second was the expansion of a gas sphere into a vacuum.

Once this was done, SPFMax was used to explore two methods for converting cylindrical columns of gas into directed thrust. The cylindrical shape was motivated by the emphasis on z-pinch experiments to be conducted in the near future at UAH, and it is not clear how such a discharge can be converted into a propulsion scheme. The two methods investigated to redirect this gas column into propulsive thrust involve expanding the gas against either a pusher plate or a hemispherical nozzle. Pusher plates have been investigated as momentum transfer mechanisms in pulsed propulsion concepts such as Project Orion. Hemispherical nozzles, by contrast, have not attracted nearly as much attention. Part of the motivation behind this work was to determine if a nozzle may in fact offer better propulsion performance than a pusher plate. The propellant plasma was

also investigated under a wide variety of geometric shapes to determine what general form would offer higher propulsion for both the nozzle and pusher plate. This work is intended to be the preliminary study from which future pulsed nozzle research can evolve.

The rest of the thesis is organized as follows. Chapter 2 is a literature review of previous research done on many different pulsed nuclear propulsion concepts. It also covers some of the mechanisms that have been explored to derive propulsive thrust from fusion propulsion, such as magnetic nozzles. Chapter 3 explains the fundamental mathematics behind smoothed particle hydrodynamics that have been implemented in SPFMax. This chapter includes using SPFMax to simulate a shock tube and the expansion of a gas sphere in a vacuum to verify the code is correctly simulating physics. Chapter 4 presents results obtained from simulations of pusher plate and a hemispherical nozzle, allowing for a comparison to be made between the two systems. Finally, Chapter 5 summarizes the conclusions obtained in this thesis and outlines some of the future research that may build upon this work.

CHAPTER 2

BACKGROUND

2.1 Overview of Nuclear Propulsion Concepts

Since the discovery of the vast amounts of power offered by nuclear reactions, many concepts have been explored that seeks to wield this power to propel spacecraft. Using fission and fusion for spacecraft propulsion was envisioned as early as the 1950s [4] [5].

Figure 2.1 is presented to illustrate the advantage that these systems have over traditional chemical rockets, showing the required initial spacecraft mass and mission duration needed for a roundtrip voyage to Mars [6]. This figure clearly shows that advanced propulsion systems are very effective in reducing both the required initial mass of a spacecraft and the duration time for a given mission. Shorter mission voyages are very desirable for manned missions, as it would help to mitigate muscle and bone loss that astronauts experience in microgravity. It would also limit the amount of radiation the astronauts are exposed to, which would help to alleviate the likelihood of developing cancer [7]. Reducing the travel time between destinations will also help to enable manned interplanetary missions to become routine and economical [8] [9].

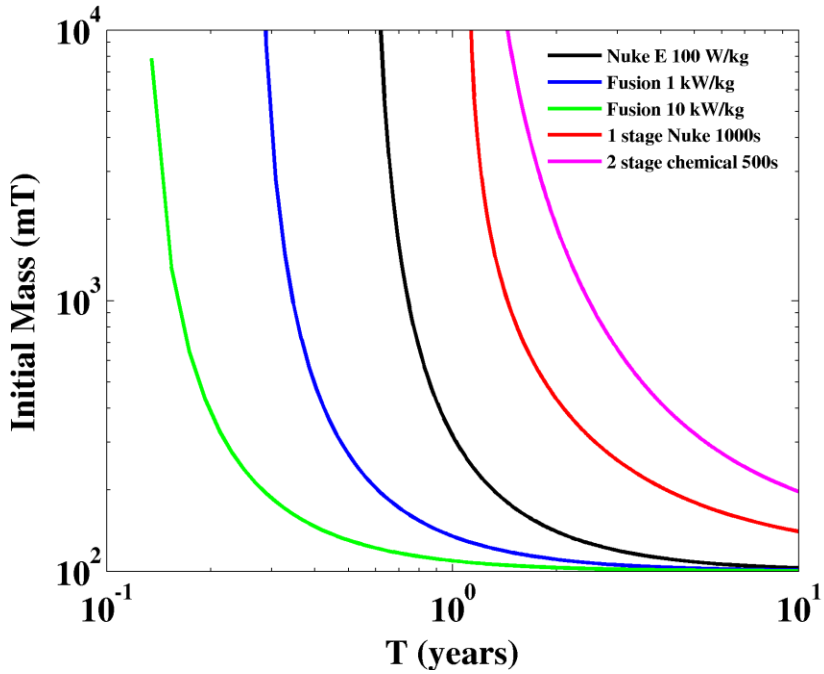

Figure 2.1 Mission requirements for different propulsion systems [6].

Many scientists and engineers have known of the great potential that nuclear propulsion offers humanity, and have sought to develop the technologies to make this a reality. One of the earliest nuclear propulsion studies conducted was Project Orion. In this concept, a spacecraft carried a large number of nuclear explosives, which would be ejected successively from the vehicle and then detonated upon reaching a specified position behind the vehicle. Plasma from the explosion would then impinge upon a pusher plate located at the spacecraft's rear, propelling the vehicle forward. To reduce the amount of acceleration subjected to the payload, a pneumatic spring system was to be used in order to provide a more gradual transmission of the momentum imparted on the pusher plate to the rest of the spacecraft [10].

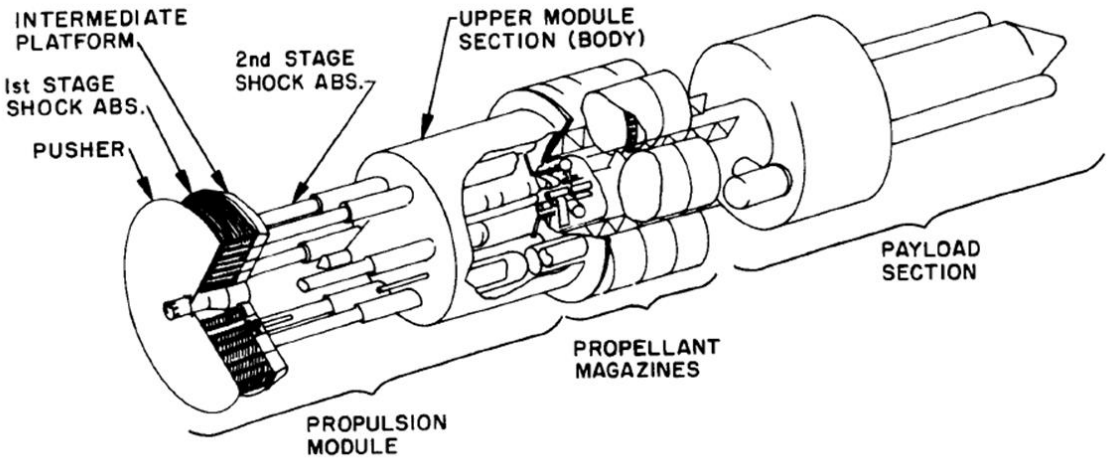

Figure 2.2 Orion spacecraft [11].

A conventional nuclear explosive radiates energy isotropically, which would result in the majority of the energy would be wasted if unmodified bombs were used to propel Orion. For this reason, a pulse unit was designed that would be far more efficient in utilizing the energy delivered by a nuclear bomb. The pulse unit consisted of a case of depleted uranium would channel the bomb's radiation into channel filler of beryllium oxide. The beryllium would capture a large amount of the bomb's energy, and then vaporize a slab of tungsten. The vaporized tungsten would then act as a propellant as it expanded into a jet of plasma which strikes the pusher plate and imparts propulsive momentum onto the spacecraft.

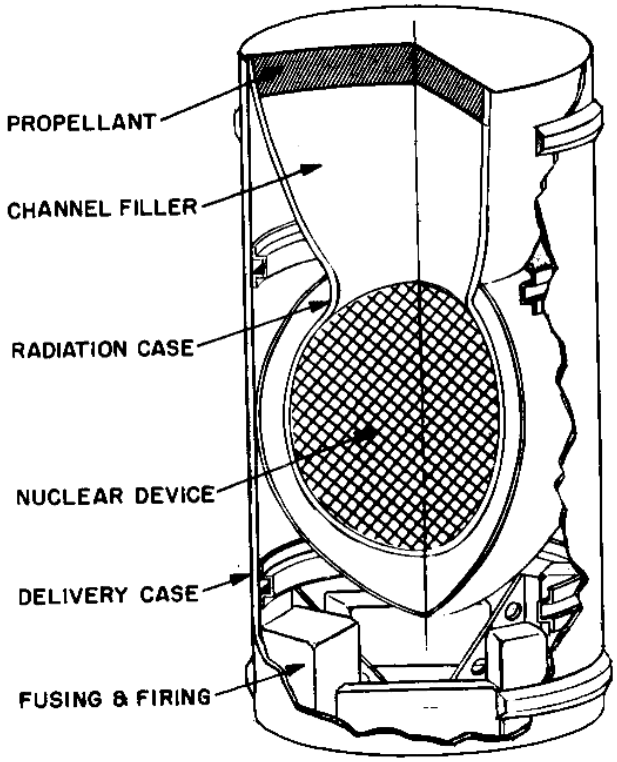

Figure 2.3 Orion pulse unit [12].

This pulse unit would allow the pusher plate to utilize 85% of the momentum the nuclear device was capable of delivering, and offered both high thrust and high specific impulse. To demonstrate the feasibility of using explosives for propulsion, the researchers constructed a one-meter diameter, 300-pound model of Orion. In the model, a series of grapefruit-sized charges of C-4 were ejected through the middle of a pusher plate at quarter-second intervals from a central stack. In 1959, a successful flight test conducted at Point Loma propelled the model to a height of about one hundred meters.

Some of the scientists that worked on Orion fully expected that they themselves would be among Orion's crew as they embarked on a grand tour of the solar system, which they viewed as being a natural extension of Charles Darwin's voyage onboard the

Beagle. This would include multi-year stays on Mars and landings on the moons of Saturn such as Enceladus.

Unfortunately, Orion was effectively killed by the Partial Nuclear Test Ban Treaty of 1963, which banned the testing of nuclear weapons underwater, in the atmosphere, and in space. However, the research conducted for Project Orion would later be used and built upon by other projects that sought to develop a myriad of nuclear propulsion concepts.

During the 1970s, research done at the Los Alamos National Laboratory investigated using a laser to initiate fusion detonations in fuel pellets [13]. The Los Alamos team also researched three different designs for systems that would convert energy from a fusion explosion into propulsive thrust. The first design was a pusher plate very similar to that which was investigated for Project Orion. For this design, a fuel pellet is detonated at a certain distance from the spacecraft and a pusher plate absorbs the shock of the explosion, imparting momentum onto the spacecraft. As with Orion, the researchers realized that ablation and spallation of the pusher plate material may have imposed performance limitations. This was addressed with the second design that the Los Alamos team investigated, which involved using superconductive coils to generate powerful magnetic field lines parallel to a conductive pusher-plate. As plasma from an explosion expands, it pushes the magnetic field lines against the pusher-plate, inducing a current in the conductive material and increasing the magnetic field strength. The increase in magnetic pressure would slow down the plasma and then accelerate it away from the pusher-plate, imparting momentum onto the spacecraft while also protecting the

pusher-plate from particle impingement. This would enable higher propellant particle velocities and a higher specific impulse than that offered by a conventional pusher-plate.

The third design investigated had the fusion detonation occurring inside a pressure vessel, with the propellant then being expelled through a conventional rocket nozzle. A number of methods exist for controlling the expansion of the fusion plasma. In one concept, the pressure vessel is filled with liquid hydrogen, and then a pulse unit is detonated at the center of the vessel. This causes a shock wave to propagate through the hydrogen until it reaches the walls of the vessel. An impulse is imparted upon the wall because the stagnation pressure at the wall is an order of magnitude higher than the frontal shock pressure. The wave is reflected back and forth between the center and the wall of the pressure vessel until equilibrium is reached, losing kinetic energy as it increases the internal energy of the hydrogen. The heated hydrogen is then expanded through the nozzle, generating thrust. Once the pressure vessel empties, it is refilled with hydrogen, and the cycle is repeated. The advantage of this system is that it would not require as much momentum conditioning as a pusher-plate. However, there are a number of disadvantages with this concept, which include a lower specific impulse and performance than that offered by a pusher-plate.

The Medusa was another nuclear propulsion concept investigated at Los Alamos by Johndale Solem in the 1990s. In this concept, a large lightweight gossamer sail in front of a spacecraft, with a long cable used to connect the two structures together. The spacecraft would then eject nuclear pulse units forward, which would detonate between itself and the sail. Material from the explosion would then impart an impulse on the sail, propelling it forward and pulling the main spacecraft along with it. The specific impulse

of Medusa was reported as being on the order of 50,000 to 100,000 seconds. An advantage Medusa has over Orion is that the sail would be far less massive than Orion's pusher plate. Another advantage is that the sail could utilize more of the pulse unit's momentum than the pusher plate [14] [15].

Research that was conducted at the Lawrence Livermore National Laboratory also investigated using laser-induced fusion microexplosions for spacecraft propulsion [16]. This design had fusion microexplosions occurring inside a thrust chamber onboard the spacecraft. A single magnetic coil would then be used to redirect the plasma from the explosions to generate the desired thrust and to avoid having the plasma come into direct contact with the structure of the vehicle. This provided a specific impulse ranging from 100,000 to 1,000,000 seconds.

Building on the research done at Lawrence Livermore National Laboratory, Hyde developed a concept for an interplanetary spacecraft that utilized laser-drive fusion with a superconducting magnet in the thrust chamber [17]. The propulsion system was assumed to have a jet efficiency of 42%, and would be capable of sending the spacecraft on a roundtrip mission to Mars in forty-five days, albeit with virtually no payload onboard. A thrust efficiency of about 65% was reported by Hyde.

Winterberg later proposed using a relativistic electron beam instead of a laser to initiate fusion microexplosions [18]. The microexplosions would occur within a concave magnetic mirror produced by superconducting magnetic fields. The specific impulse generated by this system was found to be on the order of 100,000 seconds.

The research that Winterberg conducted served as motivation for Project Daedalus, one of the most ambitious spacecraft design concepts explored. This design

study was conducted by the British Interplanetary Society in the 1970s, and the objective of the project was to design a spacecraft capable of performing a flyby mission to Bernard's Star. The propulsion system of Daedalus involved injecting fusion fuel pellets into a reaction chamber and then hitting them with powerful electron beams to initiate fusion reactions. As the fusion plasma expands, it compresses magnetic field lines within the reaction chamber, transferring kinetic energy from the plasma to the magnetic field. The field lines are compressed until the magnetic pressure is equivalent to the dynamic pressure of the plasma, after which the direction of the plasma's motion is reversed and is ejected from the reaction chamber, imparting momentum onto the spacecraft. The design of Daedalus had two propulsive stages, with each one intended to operate for about two years and have a specific impulse within the range of about 1,000,000 seconds. This would accelerate the spacecraft to about 12% of the speed of light, allowing it to reach Bernard's Star within a fifty-year timeframe [19].

A similar study conducted by NASA and the US Naval Academy was Project Longshot. The objective of this study was to design an unmanned probe capable of rendezvousing with the Alpha Centauri system within a one-hundred year timeframe. A long-life fission reactor capable of generating 300 kilowatts would be used to power the spacecraft's systems, as well as start and restart the fusion reactions. Like Daedalus, the propulsion system of Longshot also involved igniting a fusion fuel pellet with high-energy particle beams, with the resulting fusion plasma being magnetically channeled out of a nozzle to generate thrust. The specific impulse was also expected to be on the order of 1,000,000 seconds [20].

Project Icarus is an ongoing project building upon the research that was done for Daedalus. Like Daedalus, the objective of Icarus is to send an unmanned probe another star within a one hundred year timeframe, and possibly to even more remote destinations than Bernard's Star, such as Epsilon Eridani [21]. Extremely bold mission architecture for Icarus envisions the spacecraft rendezvousing with another star system and then returning to Earth using an antimatter propulsion system [22]. A somewhat less ambitious propulsion system being investigated as the primary propulsion system for Icarus is plasma jet driven magneto-inertial fusion (PJMIF). In PJMIF, converging plasma jets are launched from symmetrically distributed plasma rail guns. As the jets converge, they form a plasma liner that compresses a plasmoiod target that achieves fusion at peak compression. The fusion plasma than expands and is ejected out of a magnetic nozzle to generate thrust. The benefit of PJMIF is that it may offer higher efficiencies than magnetic confinement and inertial confinement methods to achieve fusion. This is due to the fact that as the target plasmoid compresses, the magnetic flux increases inversely proportional to the radius of the target [23].

The VISTA concept, explored by Orth at Lawrence Livermore National Laboratory, was a spacecraft intended to be used for a 145 day roundtrip manned voyage to Mars with a payload mass of 100 mT. The propulsion system of VISTA also utilized a laser to initiate fusion microexplosions, and a thrust chamber with two magnetic coils. Once injected into the thrust chamber, deuterium-tritium fuel capsules would be ignited with a 5 MJ laser, with the energy released being 200 to 1,500 times greater than the energy of the laser. Half of the fusion energy released would be in the form of neutrons, one-fourth in the form of X-rays, and one-fourth in the form of charged plasma debris.

Only the plasma debris can be used for propulsion, and consequently, only about 9% of the total energy produced would be used for propulsion. The specific impulse of VISTA was on the order of 17,000 seconds, and had a thrust efficiency of about 60% [24].

Thio et al investigated using plasma-jet driven magnetized target fusion for spacecraft propulsion [25]. In this concept, a pair of conical theta pinch coils is used to create magnetized target plasma. A spherically converging plasma liner formed from the merging of plasma jets is used to implode the plasma until a thermonuclear reaction occurs. The high pressure created by the fusion reaction compresses the liner until a thin layer of it undergoes fusion ignition. An advantage of this system is that the outer layer of the liner carries hydrogen, which can transfer a large amount of the neutron energy to charged particles that can then be expelled from a magnetic nozzle for propulsion. The engine designed had a specific impulse of 77,000 seconds and a nozzle efficiency of 80%.

The HOPE study conducted by Adams et al focused on the conceptual design of a manned vehicle capable of making roundtrip voyages to the outer solar system. The propulsion system utilized magnetized target fusion to ignite deuterium-tritium fuel pellets. The specific impulse reported was on the order of 70,000 seconds [26].

The FIREBALL (Fusion Ignition Rocket Engine with Ballistic Ablative Lithium Liner) concept explored by Martin et al at Marshall Space Flight Center [27] is a two-stage, direct-drive fission/fusion propulsion system intended to be used by an Orion-like spacecraft, Figure 2.4. Like Orion, the propulsion system consists primarily of a pusher-plate, shock absorbers, and a magazine of pulse-units.

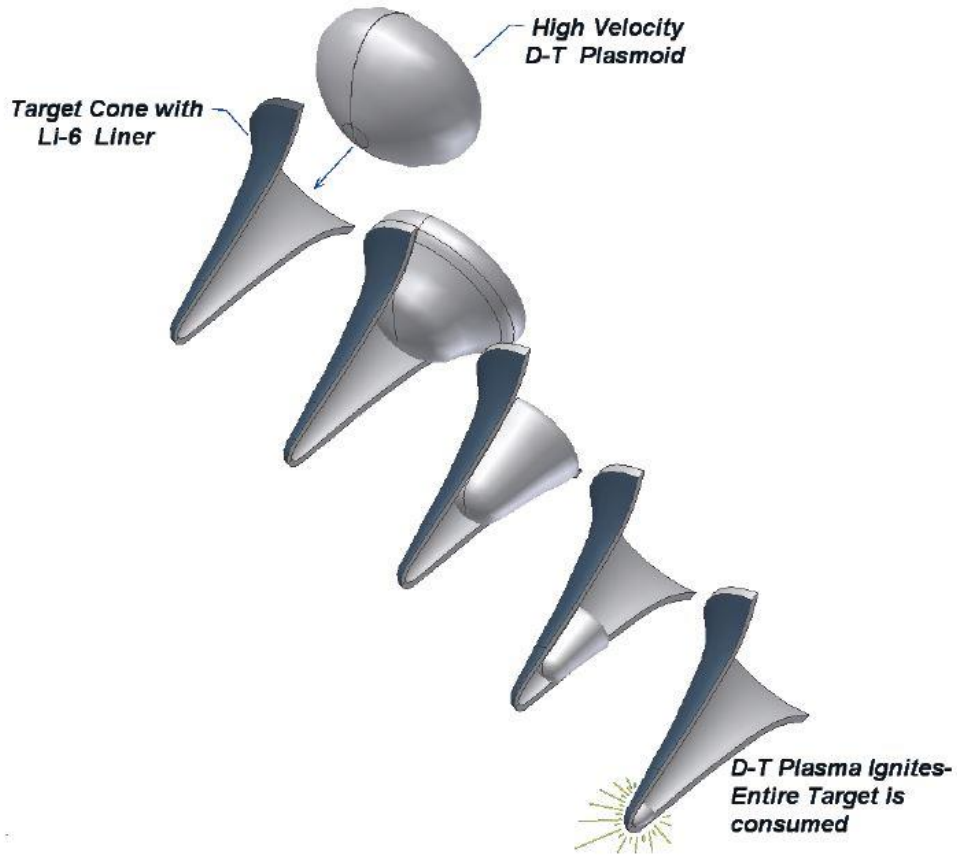

Figure 2.4. Illustration of Collision of FRC Plasmoid with the Liner [27].

To propel the FIREBALL spacecraft, a pulse unit lined with metallic lithium is launched behind the vehicle. The lithium acts as a flux conserver and confinement wall. When the pulse unit reaches a given point behind the spacecraft, a dense field revered configuration (FRC) plasmoid consisting of deuterium and tritium is launched through a multi-stage inductive accelerator and collides with the liner. The liner slows down the FRC, causing it to compress and heat the plasma until a thermonuclear reaction occurs. Fusion products produced in the plasma serve as an ignition source for the linear. As with Orion, the resulting debris impinges upon a pusher plate and imparts propulsive momentum onto the vehicle. This system offers several advantages over the original

Orion concept, one being that the pulse units do not have a fission trigger. The pulse units may also be designed to offer smaller yields than those offered by fission explosives, and are also completely passive when kept in storage.

2.2 Overview of Magnetic Nozzle Concepts

Many propulsion systems that use high-temperature plasmas also utilize magnetic nozzles to redirect the plasma in order to generate thrust. Part of the reason for this is because hot plasma can cause severe damage to many materials [28]. Utilizing magnetic fields can impede this damage from occurring by preventing the plasma from coming into physical contact with the solid-state components of the propulsion system. For magnetic nozzles to function properly, it is crucial that the plasma detaches from the nozzle's magnetic field lines, or else the plasma can be pulled back to the spacecraft and cause drag rather than impart a momentum transfer [29].

Loss mechanisms that can reduce jet power include hydrodynamic losses caused by imperfect collimations of the plasma exhaust. The magnetic field can also diffuse into the plasma prior to decoupling, which can cause the plasma to lose its conductivity. This plasma may be ejected from the nozzle in arbitrary directions due to ambipolar diffusion, while some may even become trapped within the nozzle's magnetic fields, unable to escape.

The type of magnetic nozzle depends on the confinement concept used to contain the high temperature plasma. These can be classified as two general types: steady-state and pulsed systems.

2.2.1 Steady-State Magnetic Nozzles

Steady-state systems confine high energy density plasma at high temperatures for relatively long periods of time. In a steady-state magnetic nozzle, the magnetic field lines mimic the geometric shape of a conventional converging-diverging nozzle [30]. This causes the plasma to choke at the nozzle's throat and then expand supersonically as it enters the nozzle's diverging section.

Steady-state magnetic nozzles have been used in many different electric propulsion systems, such as Hall effect thrusters and magnetoplasmadynamic thrusters [31]. One prominent example of this is the Variable Specific Impulse Magnetoplasma Rocket (VASIMR). In the VASIMR engine, propellant is ionized by an RF antenna. The cold plasma is then accelerated along converging magnetic field lines to a second RF antenna. The radio waves from the second RF antenna impact the propellant ions and electrons at resonance, causing the plasma to accelerate and achieve a much higher temperature. As the magnetic field lines diverge, the spiral paths of the ions elongate, causing them to accelerate and generate sufficient thrust for propulsion [32] [33] [34]. This is shown in Figure 2.5:

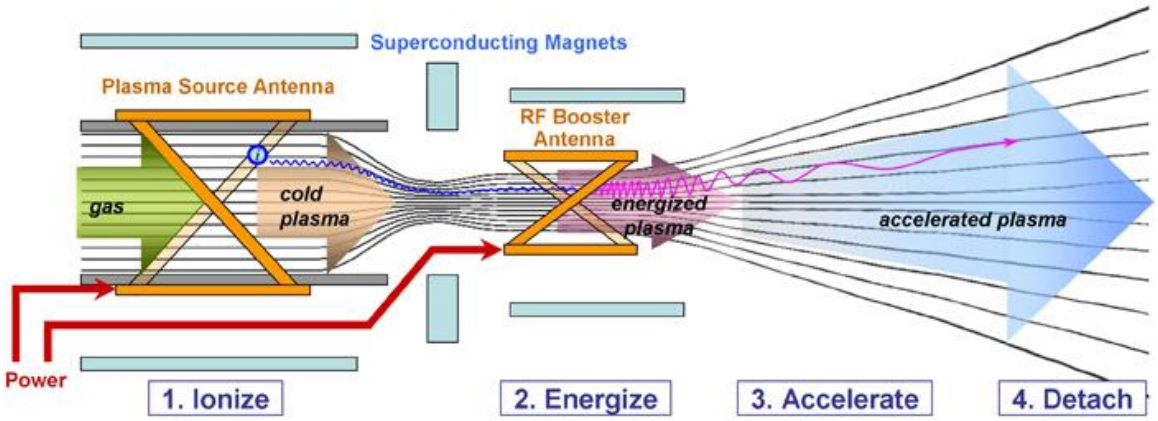

Figure 2.5. VASIMR Engine [35].

Mikellides et al. conducted numerical simulations to study the flow of plasma that would be generated at the edge of a fusion reactor and to accelerate the plasma using a magnetic nozzle. The MACH2 MHD code was used to conduct these simulations. This code is time-dependent and non-ideal, and solved dynamic, single-fluid MHD equations in two dimensions. Numerical simulations were performed to validate quasi-steady magnetic nozzle operation. In the simulations, helium plasma was decelerated to a stagnation temperature of about 100 eV and a stagnation density of about 5 x 10^{-5} kg/m^3 as it passed through a magnetic cusp, and then expanded nearly isentropically through a magnetic nozzle to reach an exhaust Mach number of 3.4. Additional simulations were conducted with the plasma at higher stagnation temperatures, which helped verify that the magnetic nozzle was operating in a manner comparable to a solid-stage converging-diverging nozzle. These simulations also provided insight into the interactions between the plasma and the magnetic field drove the formation of the current layer, and found substantial penetration of mass flux into the current layer was caused by non-uniformities

in the magnetic field. Cross-field mass transport was also observed to occur near the nozzle's exit as the plasma escaped from the axial flow to follow the radially diverging magnetic field, which caused a 24% loss of ideal thrust [36] [37].

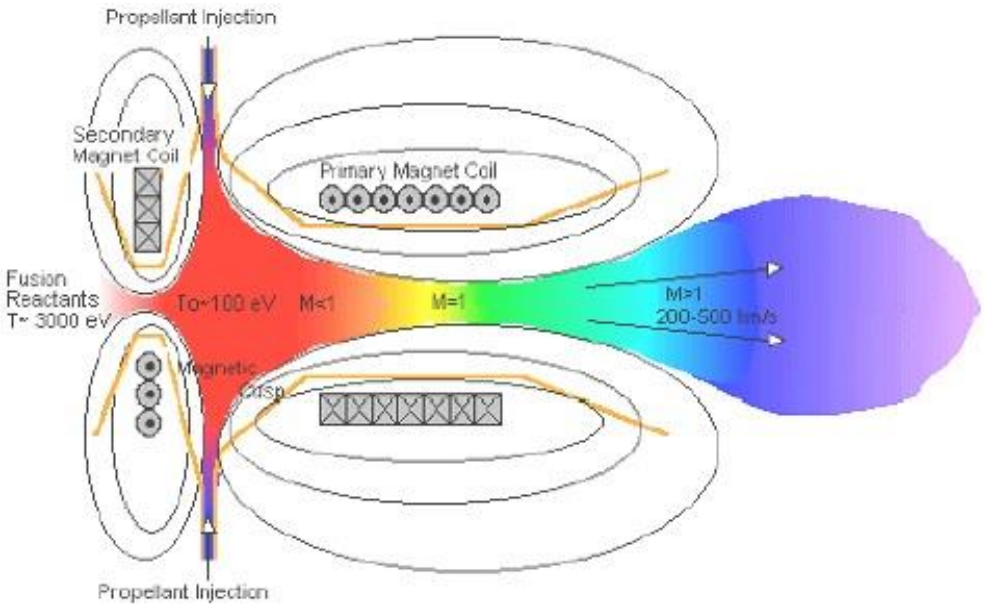

Figure 2.6. Steady-state fusion propulsion concept [37].

Gilland et al. [38] expanded upon the research conducted by Mikellides et al. by finding that the timing of plasma injection and energizing of the magnetic coils were vital parameters in optimizing the flow of the plasma. It was also found that a conical cathode provided more efficient compression of the flow than a cylindrical cathode did. In addition to this, a magnetoplasmadynamic plasma accelerator was constructed and operated at currents up to 300 kA and power levels up to 200 MW. The intention is to eventually use this facility to provide experimental verification of the computational modeling.

2.2.2 Pulsed Magnetic Nozzles

Pulsed fusion systems contain plasma for relatively brief periods of time, usually on the order of a few microseconds. In a pulsed magnetic nozzle, magnetic field lines absorb the kinetic energy of an expanding plasma sphere. The field lines are compressed until the magnetic pressure is equivalent to the dynamic pressure of the plasma. The plasma is then ejected from the nozzle as the magnetic field rebounds to its initial position [24]. This is illustrated in the figure below:

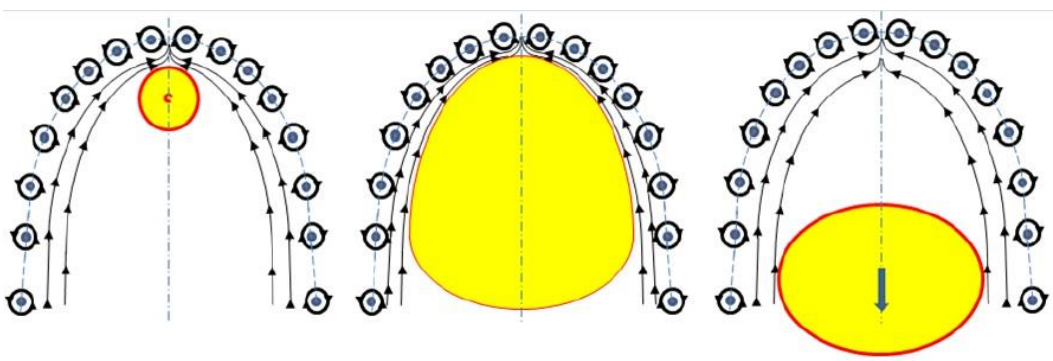

Figure 2.7. Pulsed magnetic nozzle operation [6].

Recuperating currents are also generated by the expanding plasma, which can be used to recharge the nozzle system for the next cycle [39].

In the VISTA concept, the thrust chamber is defined by the envelope of particle trajectories that the target debris follows as it expands away from the firing position and compresses the magnetic field. When the magnetic field rebounds, the plasma debris is ejected from the thrust chamber and generates a pulse of thrust that has an effective interaction time with the spacecraft of roughly 50 μs [24].

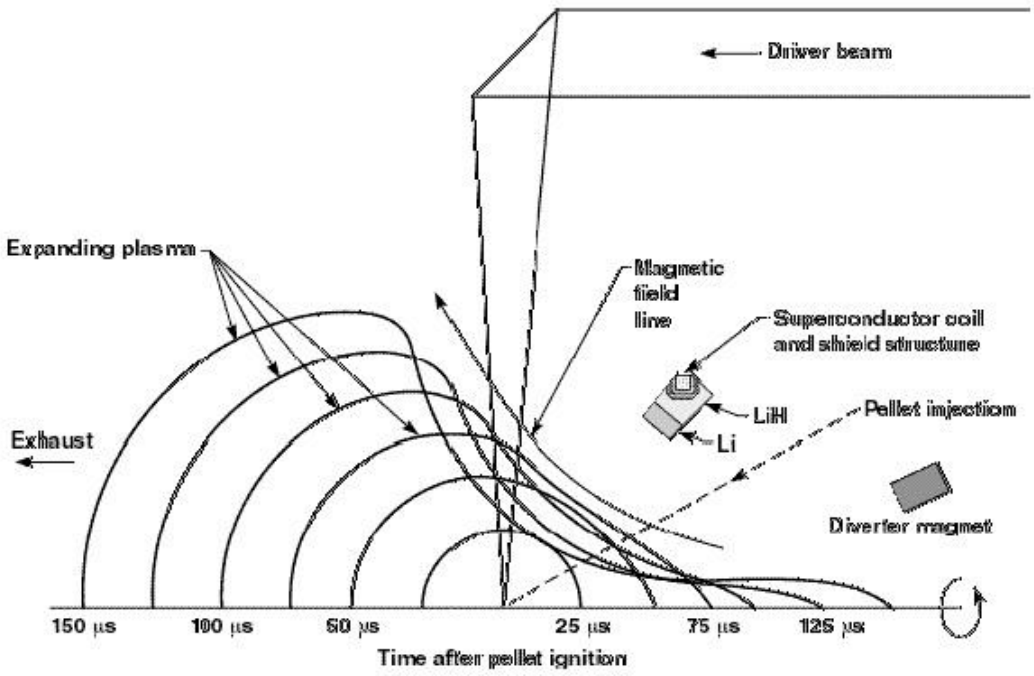

Figure 2.8 VISTA magnetic thrust chamber operation [24].

Nagamine and Nakashima used a 3D hybrid particle-in-cell code to simulate plasma flows in a single coil magnetic nozzle [40]. They found that the plasma instabilities had no serious effects on the thrust efficiency, which was determined to be about 65%.

Sakaguchi et al. investigated alternate nozzle configurations of a two coil magnetic nozzle to improve the thrust efficiency. By experimenting with different values for the position and current applied to the rear coil, they were able to increase the thrust efficiency to a maximum of 75% [41].

Many of these studies have had the fusion microexplosions occurring at the center axis of the nozzle. Kajimura et al. [42] researched how varying the location of the initial fusion detonation would affect the thrust efficiency. They also investigated how the thrust vector could be controlled by placing the initial fusion plasma off-axis from the

coil on a range from 0° to 45°. The first investigated using a single coil that had a radius of one meter, a current of 3.57 MA, and a plasma energy of 4 MJ. They were able to achieving a steering angle range from 0° to about 77°, and a thrust efficiency ranging from 50% to about 68%. They also investigated a two coil magnetic nozzle, and found that applying a current of 0.595 MA to the rear coil and positioning the initial plasma blob at the center of the rear coil yielded a maximum thrust efficiency of 78%. Tilting the rear coil was used to control the thrust vector, but only offered a steering angle range from 0° to about 5° when the rear coil was tilted from a range of 0° to 45°.

Matsuda et al. investigated improving thrust efficiency by surrounding a fusion pellet with a propellant modulator. The modulator is shaped by cutting the part that is in the direction of the magnetic nozzle. When a laser is used to initiate fusion, the modulator causes the fusion plasma to move in the direction of the coils with greater efficiency. They also investiaged using rectangular coils for both thrust vector control and improved efficiency, and were able to achieve a maximum thrust efficiency of 75% [43].

The research conducted by Maeno et al. is distinguished from many of the other studies because it involved experimentation as opposed to consisting almost entirely of simulations [44]. The apparatus for these experiments consisted of a single-beam Nd: YAG laser, a polystyrene fuel pellet, and a neodymium permanent magnet. The lases were examined at energies of 0.7 J, 1 J, and 1.5 J. The fuel pellets had diameters of 100 micrometers and 300 micrometers. The distance between the magnet and the laser beam was 10 mm, and the angle between them was 45°. The experiments were conducted at the Extreme Ultra-Violet Database laser facility at the Institute of Laser Engineering, and

investigated measured plasma emission distribution, the magnetic field strength history, and the impulse bit. The plasma generated was observed being pushed along the magnetic field lines in the manner of a magnetic nozzle, and the maximum impulse bit was found to be about 2 μNs.

Parabolic nozzle configurations using more than two coils have been explored by Thio et al [25]. and Adams et al [26]. In this concept, the fusion detonations occur at the focus of a coil parabola of magnetic coils. The studies reported this concept to have a theoretical thrust efficiency of 86%.

2.3 Solid-State Pulsed Nozzles

It is worth noting that research on solid-state hemispherical nozzles are lacking in the literature. Concepts such as the magnetic nozzle in the Hope study did utilize a solid-state parabolic-shaped nozzle, but this included the utilization of magnetic coils. The main advantage that solid-state systems have over magnetic nozzles is simplicity. For the first generation of spacecraft utilizing pulsed nuclear propulsion systems, simplicity will likely be a major deciding factor in the design process. Other issues that arise from the utilization of pulsed solid-state systems, such as ablation and material failure, will be left to future research.

The lack of research in the performance of a solid-state hemispherical nozzle provided further motivation to simulate such a system for this thesis. Comparing such a nozzle to other systems is vital for determining how a future propulsion system should be designed. Studying the effects of initial conditions on nozzle performance can be used to identify critical issues for achieving high propulsion efficiency that may lead to better

insights in the design of more complicated systems that may include pulsed magnetic nozzles.

CHAPTER 3

SPFMax

3.1 Introduction

Many problems in engineering are in the form of partial differential equations (PDEs) of field variables. Analytical solutions for these equations often do not exist, making it necessary to implement numerical solutions. In order to do this, the problem domain in which the PDEs are defined must be discretized. A method is then needed that can provide an approximation for the values of the field functions and their derivatives at a given point. Obtaining numerical calculations of PDEs has been dominated primarily by grid-based finite difference methods. In finite difference methods, the interpolation points consist of the vertices of a mesh.

In contrast to this, the SPFMax code developed at the University of Alabama in Huntsville utilizes smoothed particle hydrodynamics (SPH). This method uses particles as the interpolation points and does not require a mesh. The methodology used in the implementation of SPH and the advantages that it has over finite difference methods will be elaborated on later in this chapter.

3.2 Distmesh

Geometric shapes used for the simulations in this study were created using the distmesh algorithm, a mesh generator developed by Persson and Strang [45]. In the distmesh algorithm, a signed distance function is used to define the geometry, with negative values located within a volume, and positive values located outside of a volume. A mesh is generated by using an analogy between a simplex mesh and a truss structure. The Delaunay algorithm is used to triangulate any set of points in the model, in which the points correspond to nodes of the truss, and the edges of the triangles correspond to bars. Each of the bars has a force-displacement relationship that is dependent on the current length of the bar and its initial length. Forces cause the nodes to move, and the Delaunay triangulation algorithm adjusts the topology. External forces acting on the structure come at each of the boundary nodes. This causes reaction forces to act normal to the boundary, and the magnitude of this force is just large enough to keep the nodes from moving outside. Static force equilibrium is used to determine the positions of the joints, which provides a well-shaped triangular mesh [46] [45]. Utilizing distmesh enables new nozzles to be created and simulated rapidly, a valuable capability when designing a propulsion system.

While using a mesh to create geometries would seem to be completely counterintuitive to SPH methodologies, the meshes are not being used in any of the simulation's calculations. Rather, the meshes provide initial positions for the particles in the simulation.

3.3 Smoothed Particle Hydrodynamics

Smoothed particle hydrodynamics (SPH) is a meshless Lagrangian method for computing fluid flows that was developed to study astrophysical phenomena such as star formation and supernovae [47] [48]. It begins by dividing a fluid into a set of particles. A kernel function is then used to calculate the properties for each of these particles by adding up the properties of the particles that lie within the kernel. The properties that are assigned to a specific particle are determined based on the density and proximity of other nearby particles [49] [50] [51].

For the kernel approximation, an integral interpolant can be used to obtain the value for any property in a fluid, and is defined as [52]:

$$A(r) = \int A(r')\delta(r - r')dr' \tag{3.1}$$

The Dirac delta function is given by:

$$\delta(r - r') = \begin{cases} 1 & r = r' \\ 0 & r \neq r' \end{cases} \tag{3.2}$$

By replacing the Dirac delta function with a smoothing function, the kernel approximation can be expressed as:

$$A(r) = \int A(r')W(r - r', h)dr' \tag{3.3}$$

The smoothing function is required to meet several conditions. The first is the normalization condition, which can be expressed as:

$$\int W(r - r', h)dr' = 1 \tag{3.4}$$

The second condition is the Delta function property, given by:

$$\lim_{h \to 0} W(r - r', h) = \delta(r - r') \tag{3.5}$$

The third condition is the compact condition, and is given by:

$$W(r - r', h) = 0 \;\; when \; |r - r'| > \kappa h \tag{3.6}$$

After the kernel function has been applied, the particle approximation is utilized. In the particle approximation, the system is represented by a finite number of particles characterized by a specific mass and location. The continuous integral representations in the kernel approximation are converted to discretized forms of summation over all of the particles that lie within in the support domain. This allows the integral interpolant to be approximated with a summation interpolant given by:

$$A(r) = \sum_b m_b \frac{A_b}{\rho_b} W(r - r_b, h) \tag{3.7}$$

The spatial gradient for this quantity can be computed using the equation summation:

$$\nabla A(r) = \sum_b m_b \frac{A_b}{\rho_b} \nabla W(r - r_b, h) \tag{3.8}$$

For any modeling method to accurately simulate real world physics, it must retain consistency. A finite difference method is consistent if the limit of the solution approaches an exact solution as the number of grid points approaches infinity and the mesh size approaches zero. In order for the kernel approximation to retain consistency, it must retain both constant consistency and linear consistency.

For a constant field function to be calculated exactly by the kernel approximation, the normalization condition must be met. This allows the kernel function to have zeroth-order consistency. For linear functions to be reproduced, the following condition must be met:

$$\int (r - r')W(r - r', h)dr' = 0 \tag{3.9}$$

Similar conditions must also be met in order to maintain particle consistency. The constant consistency condition is given by:

$$\sum_b W(r - r_b, h)\Delta r_b = 1 \tag{3.10}$$

The linear consistency condition is given by:

$$\sum_b (r - r_b)W(r - r_b, h)\Delta r_b = 0 \tag{3.11}$$

The particle approximation is performed at each time step, and is applied to the field functions in the partial differential equations in order to generate a set of ordinary differential equations in a discretized form with respect to time. The ordinary differential equations can then be solved using an explicit integration method. In SPFMax, a second-order Runge-Kutta method is used to integrate the equations of motion.

A cubic spline kernel function was used for the smoothing function, and is given by:

$$W_{ab} = \begin{cases} \frac{1}{4\pi {h_{ab}}^3}[(2-q)^3 - 4(1-q)^3] & for\ 0 \le q \le 1 \\ \frac{1}{4\pi {h_{ab}}^3}(2-q)^3, & for\ 1 \le q \le 2 \\ 0 & for\ q > 2 \end{cases} \tag{3.12}$$

Part of the reason this kernel function was selected is because a cubic spline has no gradients with a sign change. Other advantages that it offers include accuracy and simplicity while also having a continuous derivative.

SPH has several advantages over finite difference methods. One such advantage is that in SPH, pure advection is treated exactly. This allows the transport of particle

properties to be exact when a velocity is specified. By contrast, results given by finite difference methods can be badly corrupted if a large velocity is superposed [51]. Another advantage is that SPH can interface problems between different materials more accurately than finite difference methods. Calculations in SPH are also only done in locations where matter is present, which helps to reduce the computing power needed to solve a given problem. Constructing a mesh can also be a difficult and time-consuming process, which meshless methods like SPH are able to avoid.

3.4 Euler Equations

To simulate fluid flow, SPFMax must numerically integrate the Euler equations. By omitting viscosity and heat transfer effects, the continuity equation can be written as:

$$\frac{\partial \rho}{\partial t} + \nabla \cdot \left(\rho \vec{V}\right) = 0 \tag{3.13}$$

The momentum equation is given by:

$$\frac{\partial \left(\rho \vec{V}\right)}{\partial t} + \nabla \cdot \left(\rho \vec{V}\right)\vec{V} + \nabla p = 0 \tag{3.14}$$

The energy equation is given by:

$$\frac{\partial E}{\partial t} + \nabla \cdot \left(\vec{V}(E + p)\right) = 0 \tag{3.15}$$

3.5 Test Cases

Because SPFMax was only developed recently, it was necessary to conduct a series of test cases in order to access the accuracy of using the code to simulate real world problems. To do this, problems that have analytical solutions are compared to the numerical solutions that SPFMax provides for the same problem. Two test cases investigated for the verification process were a shock tube and the expansion of a gas sphere in a vacuum.

3.5.1 Shock Tube

In the shock tube problem [53], a diaphragm separates two regions of gas, each having constant density and pressure. Removing the diaphragm causes a discontinuity to form between the two regions, and the discontinuity then splits into three regions. In the first region, a rarefaction wave is moving to the left which has continuous fluid variables. The second region is to the right of the rarefaction tail, and extends to the location of the contact discontinuity. The velocity and pressure are continuous across the contact discontinuity, while the density and thermal energy are continuous. To the right of the contact surface is a postshock region bordered by a shock wave. There exists an analytical solution to this problem that can be used to calculate the temperature, density, and pressure at any point in time.

The accurate capturing of shocks is a vital capability for any fluid simulation code, which makes the shock tube a useful problem to analyze a code's accuracy [54]. By running this problem with a simulation code and comparing the results to the analytical solution, it can be determined if the code is converging to the correct solution.

3.5.2 Verification Procedure

To perform this analysis, it should be determined if the numerical approaches the analytical solution as the simulation's resolution increases. A sequence converges to a value of ξ with order p if it meets the following criteria:

$$|x_n - \xi| < Cn^{-p} \tag{3.16}$$

In which C is a constant and n is the number of grid points. For code verification, ξ is equal to zero, since the error should approach zero as the resolution increases [55].

Using density as an example, the error can be computed as being:

$$\rho_{error} = \frac{|\rho - \rho_{exact}|}{|\rho_{exact}|} \tag{3.17}$$

The L1 norm is then calculated using the following equation:

$$L1_{\rho} = \frac{\rho_{error}}{n} \tag{3.18}$$

The L1 norm provides a global average error. This method is used to measure the error for density, temperature, and pressure at three different resolutions. A higher resolution generates more particles, which in turn should provide a more accurate solution.

The simulation that was examined consisted of two argon blocks, each with a length of 15 centimeters and an initial number density of 10^{26}. The left block has an initial temperature of 100 eV, and the right block has an initial temperature of 10 eV.

The shock tube problem was run at three different resolutions, with the highest resolution having a total of 3,006 gas particles. A comparison between the results for the highest resolution and the analytical solution is shown in the following three figures:

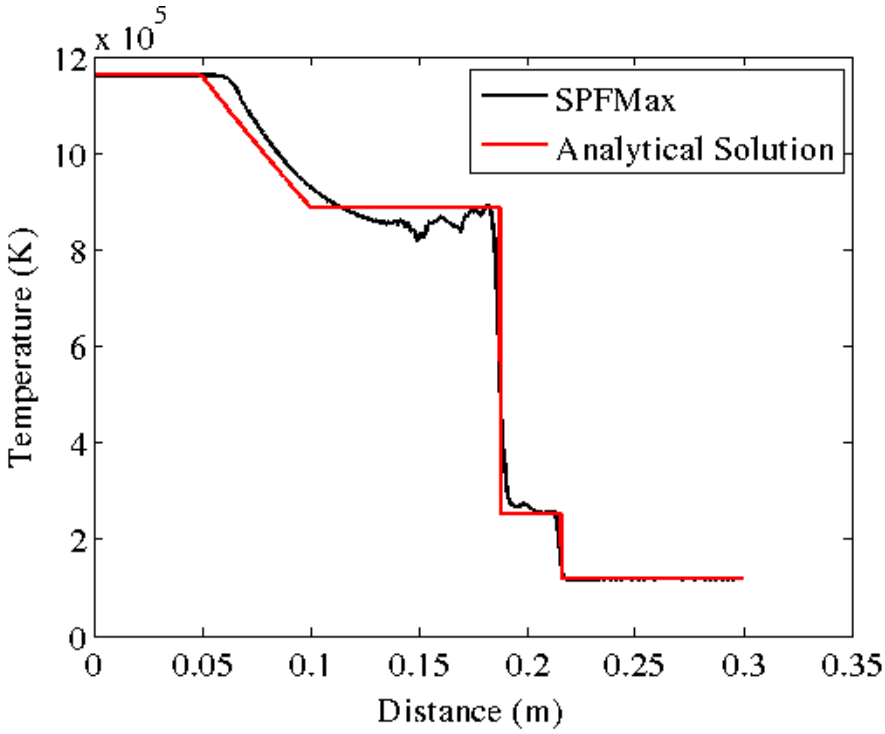

Figure 3.1 Comparison between SPFMax and analytical solution for temperature.

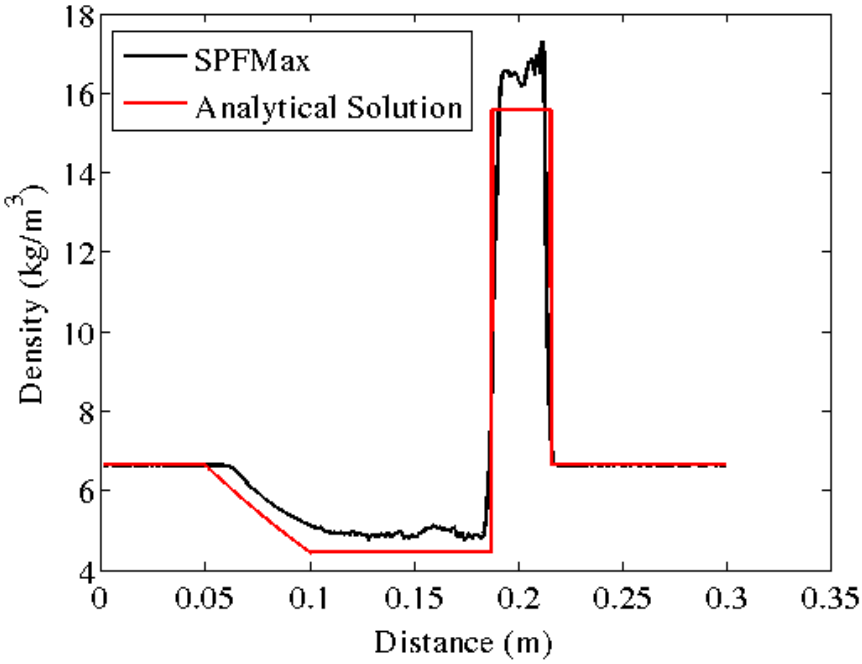

Figure 3.2 Comparison between SPFMax and analytical solution for density.

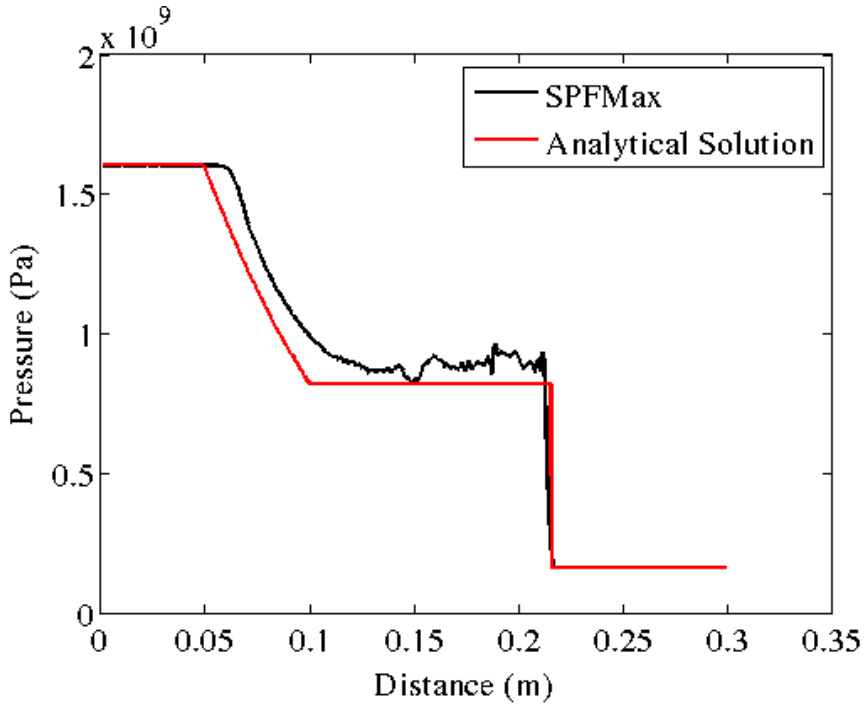

Figure 3.3 Comparison between SPFMax and analytical solution for pressure.

The lowest resolution examined had a total of 270 gas particles, and a medium resolution that was examined had a total of 900 gas particles. The L1 norms for each of the three resolutions were then graphed on log-log plots, which are shown in Figures 3.4, 3.5, and 3.6.

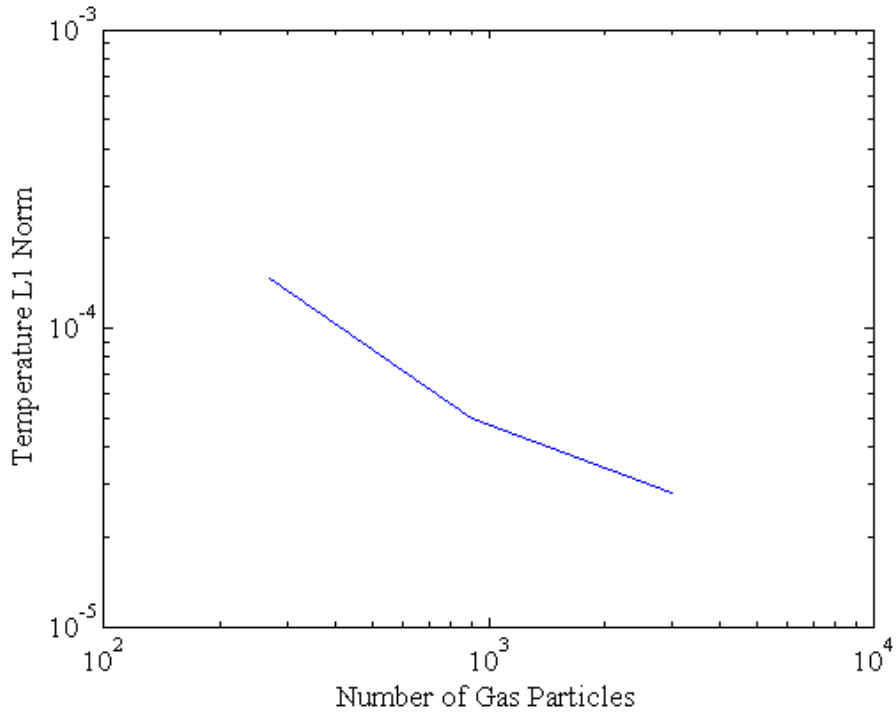

Figure 3.4 Log-log plot of temperature convergence. Slope is -0.69

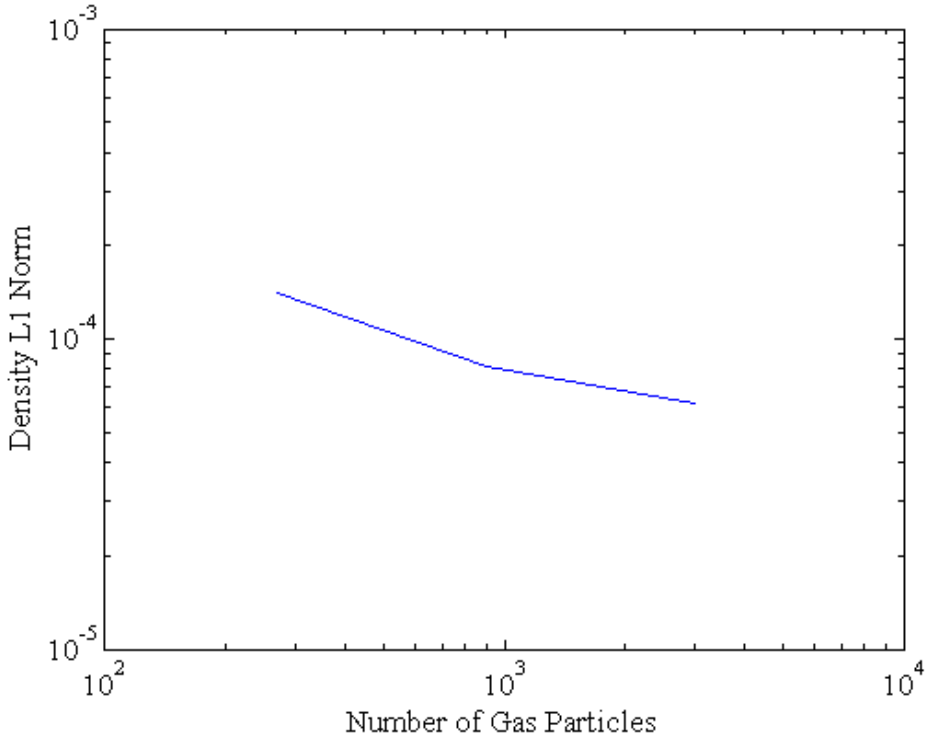

Figure 3.5 Log-log plot of density convergence. Slope is -0.3

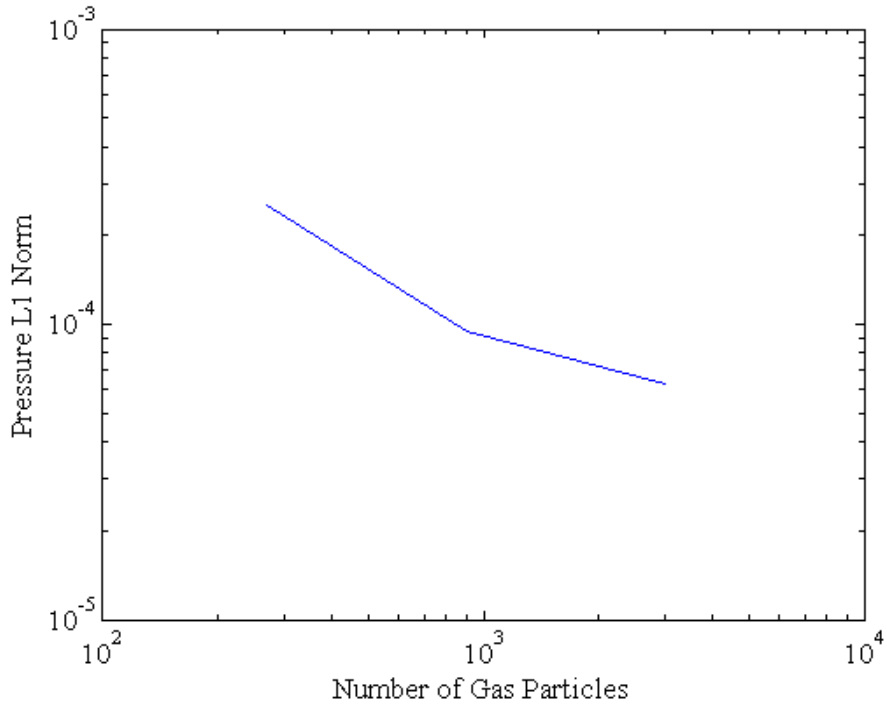

Figure 3.6 Log-log plot of pressure convergence. Slope is -0.58

The y-intercept of these plots equates to C from Equation 3.16, and the slope of the plots is equivalent to p from Equation 3.16 [55]. Based on these values, it can be concluded that the convergence rate of SPFMax is $\sim n^{0.5}$.

3.5.3 Expansion of a Gas Sphere

The expansion of a gas sphere in a vacuum is a problem very pertinent for spacecraft propulsion. If SPFMax can be shown to accurately simulate this kind of problem, it will offer much confidence that it is able to simulate the gas dynamics of plasmas.

The problem that was investigated in this case study consisted of a sphere of argon with an initial radius of five centimeters, an initial temperature of 1,000 eV, and a number density of 10^{28}. The simulation was run for a time of twenty microseconds.

Figures 3.7, 3.8, and 3.9 are presented to illustrate the expansion of the gas sphere throughout the simulation.

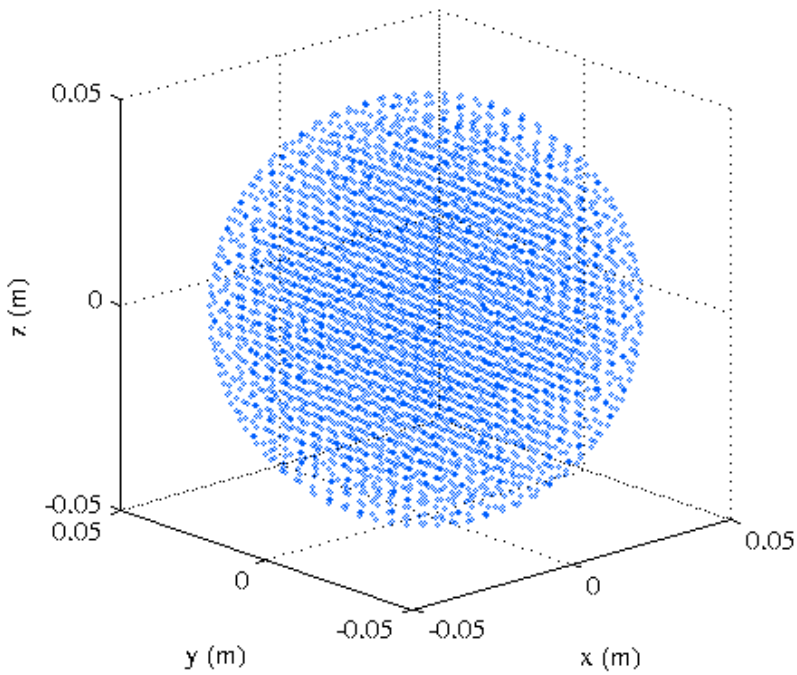

Figure 3.7 Initial gas sphere.

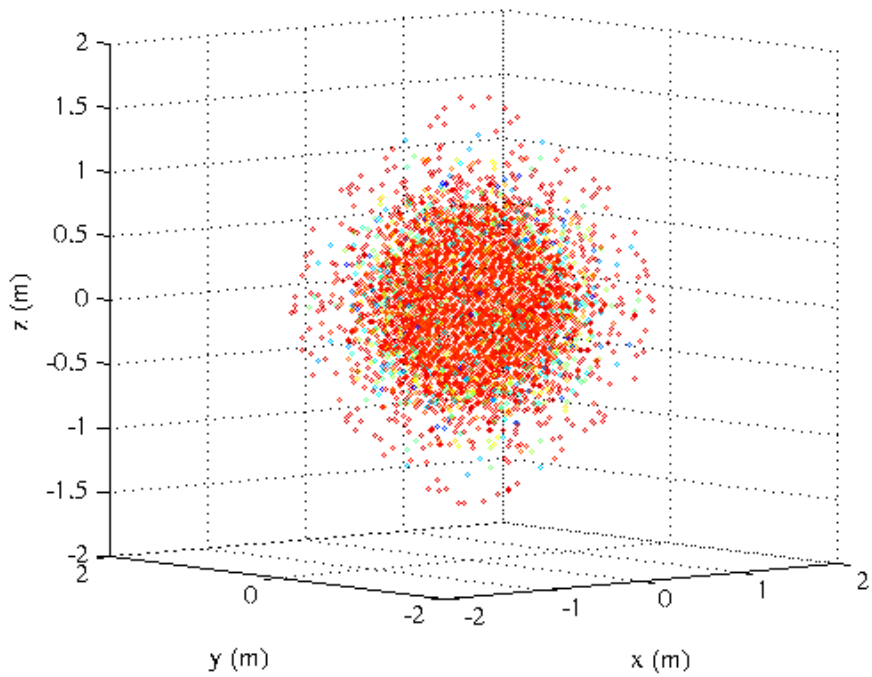

Figure 3.8 Gas sphere at 10 microseconds.

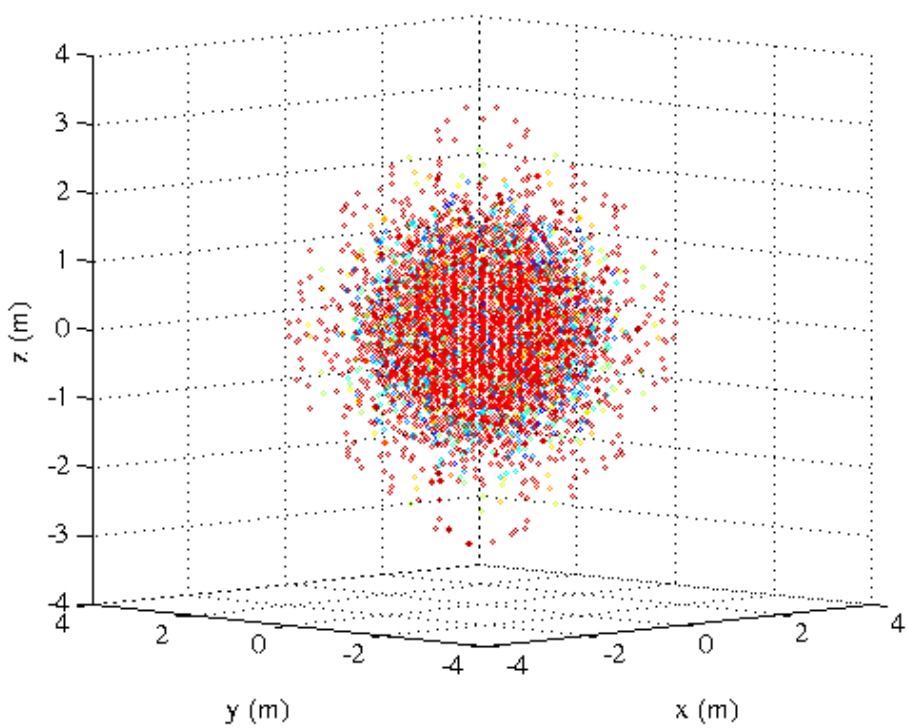

Figure 3.9 Gas sphere at 20 microseconds.

It can be seen from these figures that the gas sphere expands symmetrically throughout the simulation, as is to be expected. To further validate that gas dynamics are being simulated correctly, it was necessary to determine the velocity at which the gas expanded. Zel'dovich and Raizer found that the maximum theoretical expansion velocity of gas sphere in a vacuum is given by [56]:

$$u_{max} = \sqrt{2C_v T_0} \tag{3.19}$$

In the case investigated, the maximum theoretical expansion velocity should be 84,912 m/s. A comparison between this value and the actual expansion velocity of the gas sphere throughout the simulation is shown in the following figure:

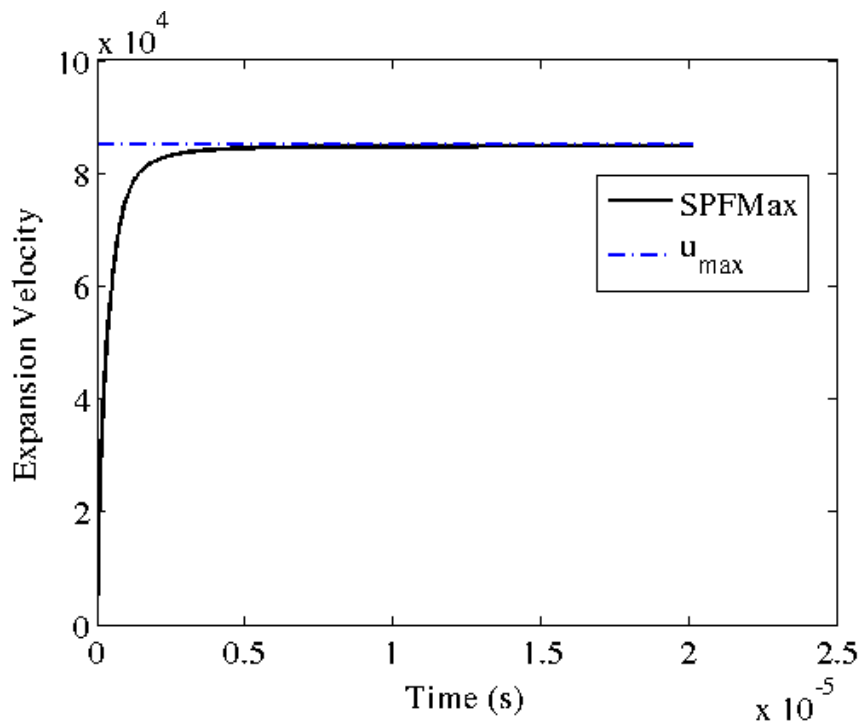

Figure 3.10 Expansion velocity of gas sphere.

In this figure it can be seen that as time progresses, the expansion velocity asymptotically approaches the maximum theoretical expansion velocity. This offers further evidence that SPFMax is correctly simulating gas dynamics.

The successful simulations of both the shock tube and the gas sphere expansion provide the verification needed to begin implementing SPFMax to simulate propulsion systems, which is the focus of the next chapter.

CHAPTER 4

PROPULSION SIMULATIONS

4.1 Introduction

The principle objective of this study was to determine the optimal shape of a propellant gas for an advanced pulsed propulsion system. Two main mechanisms were investigated: a pusher plate and a hemisphere. As seen in the literature review in Chapter 2, pusher plates have been a popular propulsion mechanism for advanced pulsed spacecraft designs. However, a hemispherical shape was also investigated to determine if it offers any performance advantages over a pusher plate.

Two figures of merit used to assess the performance of the propulsion system were the specific impulse and the propulsion efficiency. The specific impulse was obtained from the summation of the propellant momentum in the z direction divided by the product of gravity and the summation of the propellant mass as given by:

$$I_{sp} = \frac{\sum m_p v_z}{g_0 \sum m_p} \tag{4.1}$$

The propulsion efficiency was defined as being the fraction of the initial thermal energy of the plasma that is converted to kinetic energy in the positive z direction, and is given by:

$$\eta = \frac{\sum 0.5 m_p v_z^2}{E_0} \tag{4.2}$$

The values for the specific impulse and propulsion efficiency were obtained based on when the propellant gas particles exited the control volume of the propulsion system. For the hemispherical nozzle, the control volume was defined as the interior volume of the nozzle. The control volume for the pusher plate was defined as the volume initially occupied by the plasma when it is pressed against the pusher plate. Both the pusher plate and hemispherical nozzle are imparted with a propulsive momentum change when the propellant gas leaves their respective control volumes.

The propellant used in this study was a cylinder of argon plasma initially at rest. The selection of a cylindrical shape was due to the fact that such plasma shapes are being investigated for future Z-pinch experiments with high-temperature plasmas at the University of Alabama in Huntsville. Argon is also expected to be used in future propulsion experiments, which is why it was selected as the propellant of choice. These planned experiments may benefit from the work done in this thesis.

In the simulations that were conducted, the outer edge of the plasma cylinder was located at the exit of the nozzle, with the axial centers of the nozzle and cylinder coinciding with each other. A cross-sectional view illustrating the propellant within the nozzle control volume is shown in Figure 4.1.

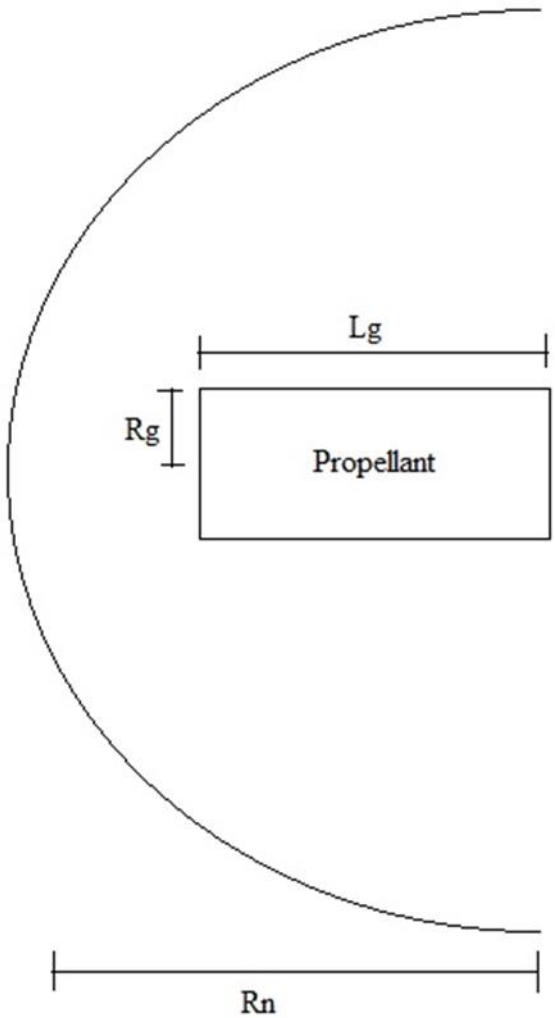

Figure 4.1 Cross-section of nozzle and propellant.

Two dimensionless geometric parameters were used to investigate what effect varying the shape of the propellant cylinder would have on the propulsion performance. The first parameter is the ratio of the gas radius to the radius of the nozzle, and is given by:

$$r_{gn} = \frac{R_g}{R_n} \tag{4.3}$$

The second parameter is the ratio of the length of the gas to the radius of the gas, and is defined as:

$$l_{gn} = \frac{L_g}{R_g} \tag{4.4}$$

By sweeping over a wide range of values for these parameters, it can be determined if the propellant cylinder should be long and thin, or short and thick, or some other permutation, as well as how large relative it should be relative to the nozzle and the pusher plate.

In order to create actual geometries that can be used in simulations, at least one geometric feature had to be defined and held constant. To meet this requirement, the propellant cylinder was given a radius of five centimeters. The selection of this small value was due primarily to limit the number of gas particles used in the simulation. While using a large number of particles could provide both a very accurate values for the figures of merit as well as simulate a propulsion system on an actual spacecraft, doing so would require a prohibitively large amount of time and computing power. In addition to this, propellant masses, nozzles, and pusher plates of comparable sizes may eventually be used in experiments to further explore the issues raised in this thesis. Once this was done, it was then possible to being shifting through the design variables to find what permutation offered higher propulsion performance.

4.2 Nozzle Performance Results

A total of fourteen nozzle geometries were created with different permutations of r_{gn} and l_{gn}. Two of these geometries are presented in Figures 4.2 and 4.3.

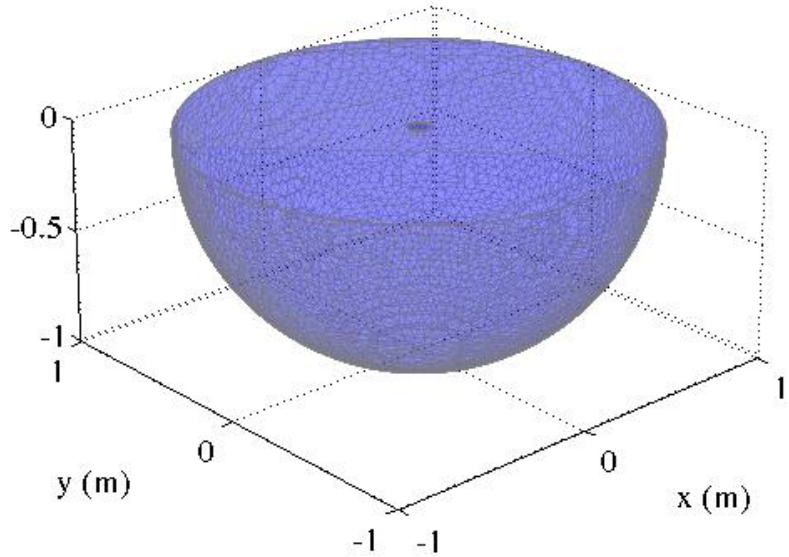

Figure 4.2 Nozzle geometry with r_{gn} of 0.05 and l_{gn} of 0.1.

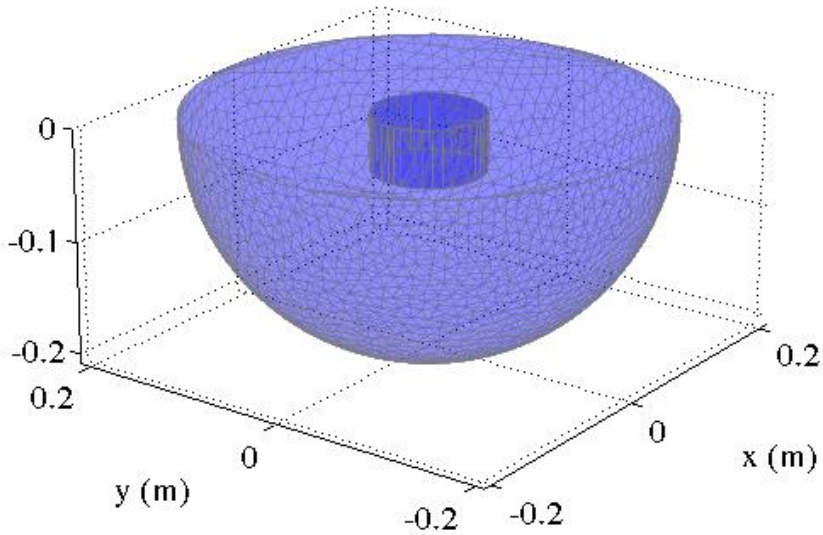

Figure 4.3 Nozzle geometry with r_{gn} of 0.25 and l_{gn} of 1.0.

Simulations were then conducted that sought to find the trends in the plasma's shape, temperature, and density that would offer high performance. Values assigned to the initial temperature of the plasma were 1 eV, 100 eV, and 1,000 eV. The number density of the plasma was given values of 10^{24}, 10^{26}, and 10^{28}. Varying these parameters lead to a total of one hundred and twenty-six permutations for the nozzle and propellant that had to be simulated. Tables 4.1-4.9 summarize the specific impulse and propulsion efficiency attained for each of these simulations.

Table 4-1 Nozzle performance at 1 eV and 10^{24} number density.

r_{gn}	l_{gn}	**Specific Impulse (s)**	**Propulsion Efficiency**
0.05	0.1	188	57.8%
0.05	0.3	181	56.9%
0.05	1.0	146	36.9%
0.05	3.0	153	38.1%
0.10	0.1	194	66.4%
0.10	0.3	194	63.1%
0.10	1.0	186	57.0%
0.10	3.0	178	54.2%
0.25	0.1	200	68.7%
0.25	0.3	196	65.1%
0.25	1.0	191	59.4%
0.50	0.1	197	66.0%
0.50	0.3	182	59.3%
1.00	0.1	210	71.8%

Table 4-2 Nozzle performance at 1 eV and 10^{26} number density.

r_{gn}	l_{gn}	Specific Impulse (s)	Propulsion Efficiency
0.05	0.1	189	58.1%
0.05	0.3	179	55.3%
0.05	1.0	149	37.1%
0.05	3.0	155	37.2%
0.10	0.1	195	65.8%
0.10	0.3	195	64.7%
0.10	1.0	188	56.9%
0.10	3.0	177	55.9%
0.25	0.1	200	69.4%
0.25	0.3	198	66.3%
0.25	1.0	195	60.5%
0.50	0.1	198	65.6%
0.50	0.3	187	61.6%
1.00	0.1	212	71.7%

Table 4-3 Nozzle performance at 1 eV and 10^{28} number density.

r_{gn}	l_{gn}	Specific Impulse (s)	Propulsion Efficiency
0.05	0.1	186	57.5%
0.05	0.3	182	56.7%
0.05	1.0	145	37.3%
0.05	3.0	156	38.3%
0.10	0.1	196	67.5%
0.10	0.3	198	65.1%
0.10	1.0	189	58.1%
0.10	3.0	179	54.5%
0.25	0.1	199	69.6%
0.25	0.3	200	67.2%
0.25	1.0	198	61.1%
0.50	0.1	197	66.2%
0.50	0.3	188	61.9%
1.00	0.1	212	72.1%

Table 4-4 Nozzle performance at 100 eV and 10^{24} number density.

r_{gn}	l_{gn}	Specific Impulse (s)	Propulsion Efficiency
0.05	0.1	1,757	57.8%
0.05	0.3	1,805	56.4%
0.05	1.0	1,458	36.9%
0.05	3.0	1,530	38.1%
0.10	0.1	1,940	66.5%
0.10	0.3	1,943	63.2%
0.10	1.0	1,864	57.0%
0.10	3.0	1,779	54.2%
0.25	0.1	1,999	68.7%
0.25	0.3	1,961	65.1%
0.25	1.0	1,904	59.5%
0.50	0.1	1,965	66.7%
0.50	0.3	1,886	59.5%
1.00	0.1	2,091	71.8%

Table 4-5 Nozzle performance at 100 eV and 10^{26} number density.

r_{gn}	l_{gn}	Specific Impulse (s)	Propulsion Efficiency
0.05	0.1	1,784	57.9%
0.05	0.3	1,815	57.3%
0.05	1.0	1,426	36.4%
0.05	3.0	1,536	38.1%
0.10	0.1	1,975	67.8%
0.10	0.3	1,974	63.7%
0.10	1.0	1,872	57.2%
0.10	3.0	1,813	53.8%
0.25	0.1	2,007	68.3%
0.25	0.3	2,000	66.3%
0.25	1.0	1,918	58.6%
0.50	0.1	1,983	67.7%
0.50	0.3	1,972	60.4%
1.00	0.1	2,094	71.8%

Table 4-6 Nozzle performance at 100 eV and 10^{28} number density.

r_{gn}	l_{gn}	Specific Impulse (s)	Propulsion Efficiency
0.05	0.1	1,767	58.9%
0.05	0.3	1,790	57.0%
0.05	1.0	1,505	38.2%
0.05	3.0	1,586	40.1%
0.10	0.1	1,954	68.9%
0.10	0.3	1,969	66.6%
0.10	1.0	1,949	58.3%
0.10	3.0	1,903	55.3%
0.25	0.1	2,006	68.8%
0.25	0.3	1,999	65.4%
0.25	1.0	1,920	59.8%
0.50	0.1	1,975	68.0%
0.50	0.3	1,960	59.4%
1.00	0.1	2,093	71.9%

Table 4-7 Nozzle performance at 1,000 eV and 10^{24} number density.

r_{gn}	l_{gn}	Specific Impulse (s)	Propulsion Efficiency
0.05	0.1	5,592	57.7%
0.05	0.3	5,672	56.5%
0.05	1.0	4,575	36.4%
0.05	3.0	4,845	38.1%
0.10	0.1	6,136	66.6%
0.10	0.3	6,202	63.5%
0.10	1.0	5,896	57.0%
0.10	3.0	5,624	54.2%
0.25	0.1	6,313	68.7%
0.25	0.3	6,158	63.9%
0.25	1.0	6,072	58.9%
0.50	0.1	6,231	66.8%
0.50	0.3	5,779	57.1%
1.00	0.1	6,622	72.3%

Table 4-8 Nozzle performance at 1,000 eV and 10^{26} number density.

r_{gn}	l_{gn}	Specific Impulse (s)	Propulsion Efficiency
0.05	0.1	5,602	58.9%
0.05	0.3	5,680	57.1%
0.05	1.0	4,552	36.3%
0.05	3.0	4,850	38.1%
0.10	0.1	6,211	66.7%
0.10	0.3	6,203	63.6%
0.10	1.0	5,902	57.2%
0.10	3.0	5,630	53.8%
0.25	0.1	6,315	69.5%
0.25	0.3	6,155	66.3%
0.25	1.0	6,069	58.6%
0.50	0.1	6,235	67.7%
0.50	0.3	5,783	58.9%
1.00	0.1	6,627	71.6%

Table 4-9. Nozzle performance at 1,000 eV and 10^{28} number density.

r_{gn}	l_{gn}	Specific Impulse (s)	Propulsion Efficiency
0.05	0.1	5,595	58.3%
0.05	0.3	5,670	57.9%
0.05	1.0	4,558	39.7%
0.05	3.0	4,855	39.8%
0.10	0.1	6,215	68.7%
0.10	0.3	6,205	65.7%
0.10	1.0	5,908	59.2%
0.10	3.0	5,650	54.1%
0.25	0.1	6,318	68.5%
0.25	0.3	6,147	65.6%
0.25	1.0	6,073	59.5%
0.50	0.1	6,245	69.2%
0.50	0.3	5,791	60.1%
1.00	0.1	6,631	71.9%

In all cases, it was found that a higher initial propellant temperature offers a higher specific impulse. This can be attributed to the fact that a higher temperature will provide the propellant gas particles with a greater amount of thermal energy, which can then be converted to kinetic energy as the gas expands against the nozzle.

For the simulations that have the same geometry and temperature, variations in the specific impulse and propulsion efficiency are observed with different permutations of number density. However, it should also be noted that these variations are within about 5% of each other. This suggests that the observed variations in specific impulse and propulsion efficiency can be attributed to an artifact of the numerical calculation and not caused by an actual physical phenomenon. This would be consistent with the Euler equations, which indicate that if the initial temperature and velocity are held constant, altering the density should not have an impact on the observed performance.

In regards to the geometric parameters, the variations in nozzle performance are too great to be attributed solely to errors in numerical integration. Therefore, it can be deduced that higher propulsion performance is offered by a large value for r_{gn} that approaches 1 and a small value for l_{gn} that approaches 0, which equates to a flat pancake-shaped propellant mass with the same diameter as the nozzle. The geometric permutation with the closest values to this had an r_{gn} of 1 and an l_{gn} of 0.1. The model for this particular nozzle and propellant shape is provided in Figure 4.4:

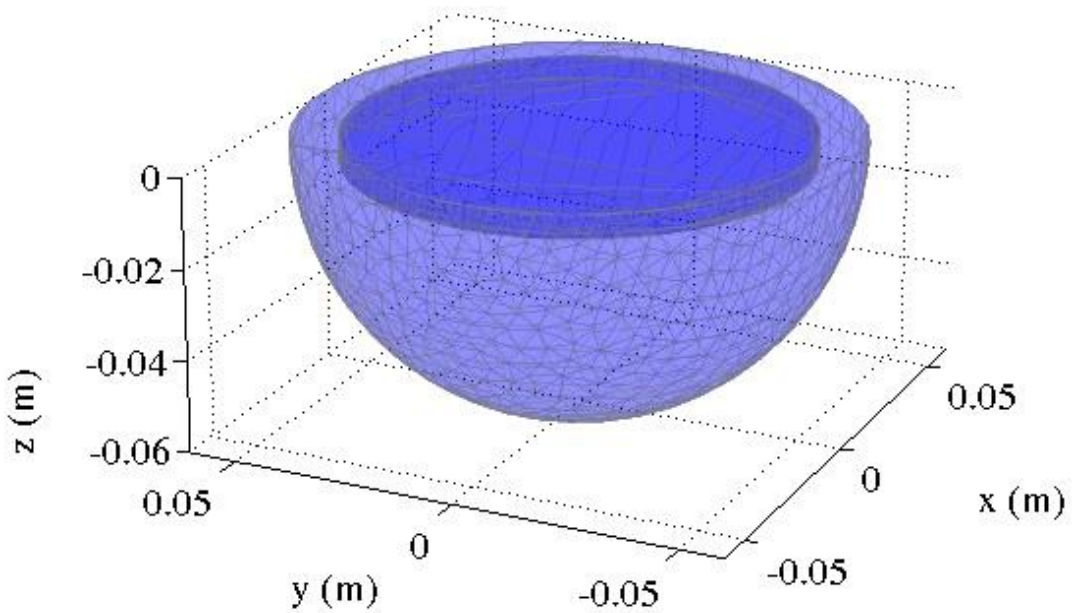

Figure 4.4 Nozzle with pancake-shaped propellant mass.

To better illustrate the operation for this particular geometry, one of the nozzle simulations will now be presented in greater detail. In this case, the propellant has an initial temperature of 1,000 eV and a number density of 10^{26}. Figures 4.6 and 4.7 depict the time evolution of this nozzle's specific impulse and propulsion efficiency throughout the simulation.

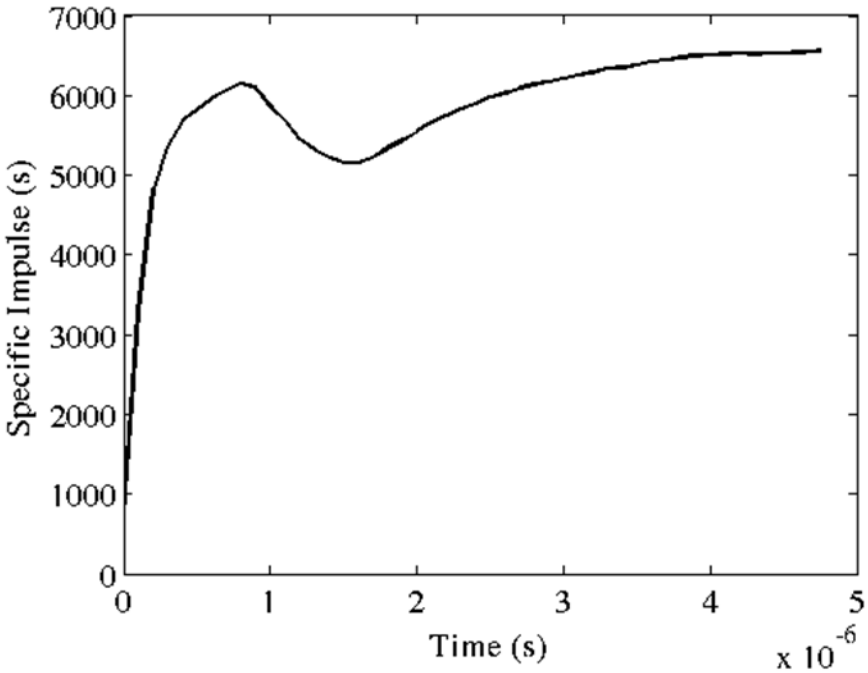

Figure 4.5 Nozzle specific impulse.

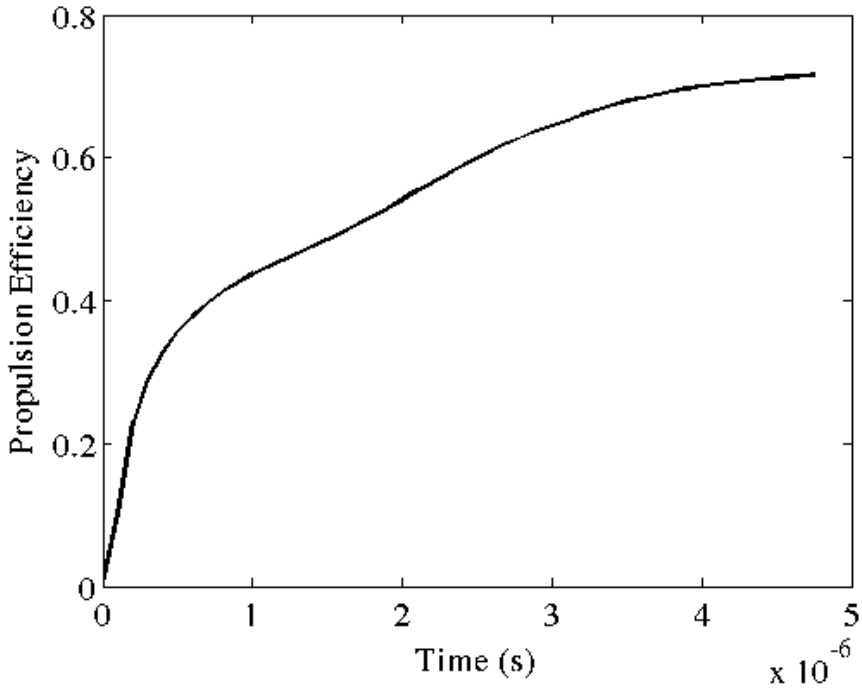

Figure 4.6 Nozzle propulsion efficiency.

Figure 4.7 shows propellant gas particles being ejected from the nozzle during the simulation. The image was taken at a simulation time of about 0.84 microseconds, which corresponds to the first peak observed in the specific impulse in Figure 4.5. The specific impulse at this time is 6,176 seconds.

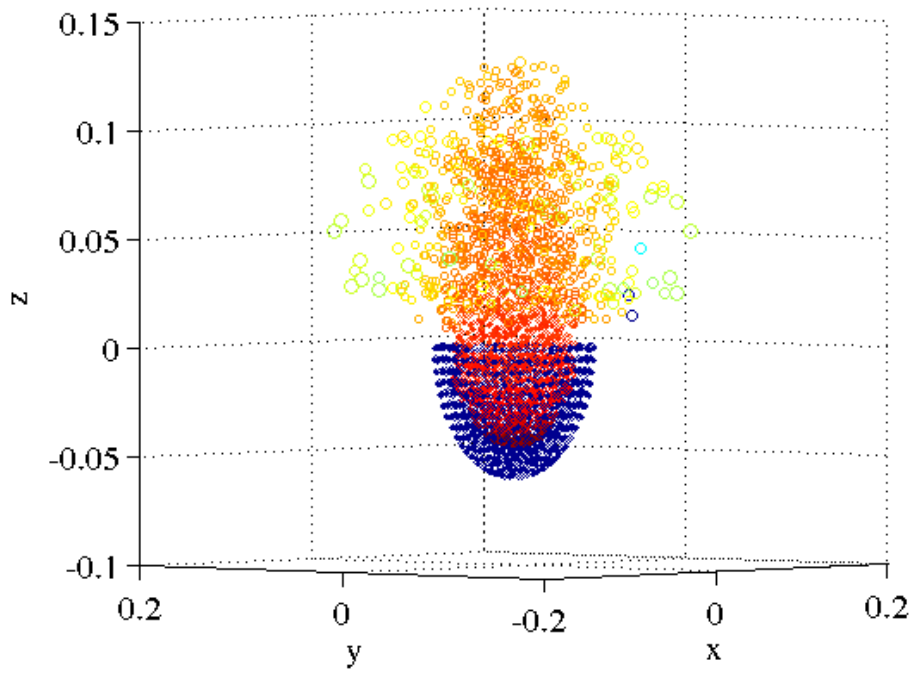

Figure 4.7 Propellant ejection from nozzle at 0.84 microseconds.

In this figure, it can be seen that a significant amount of the propellant gas particles are filling the interior volume of the nozzle as they move toward the far end of the nozzle.

Figure 4.8 was taken at a simulation time of 1.5 microseconds, corresponding to the bottom of the trough observed in the specific impulse in Figure 4.5. The specific impulse at this time is 5,151 seconds.

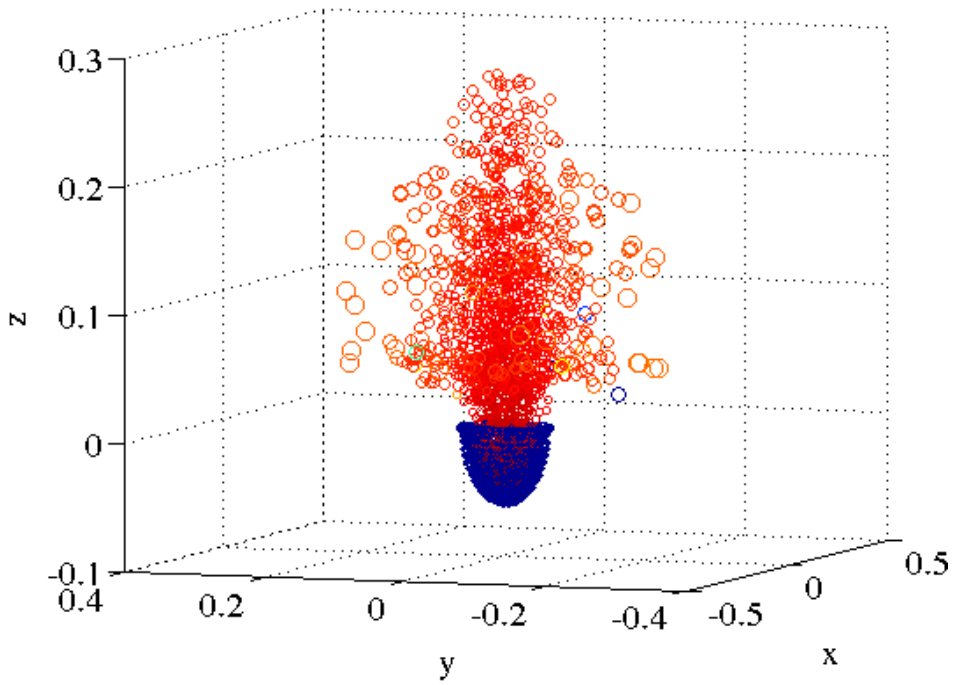

Figure 4.8 Propellant ejection from nozzle at 1.5 microseconds.

In this figure, it can be seen that much of the propellant gas particles are being ejected from the nozzle control volume, and that the particles within the nozzle are rebounding off of the wall of the nozzle.

Figure 4.9 was taken at a simulation time of about 4.7 microseconds, at which point more than 95% of the propellant has been ejected from the nozzle control volume.

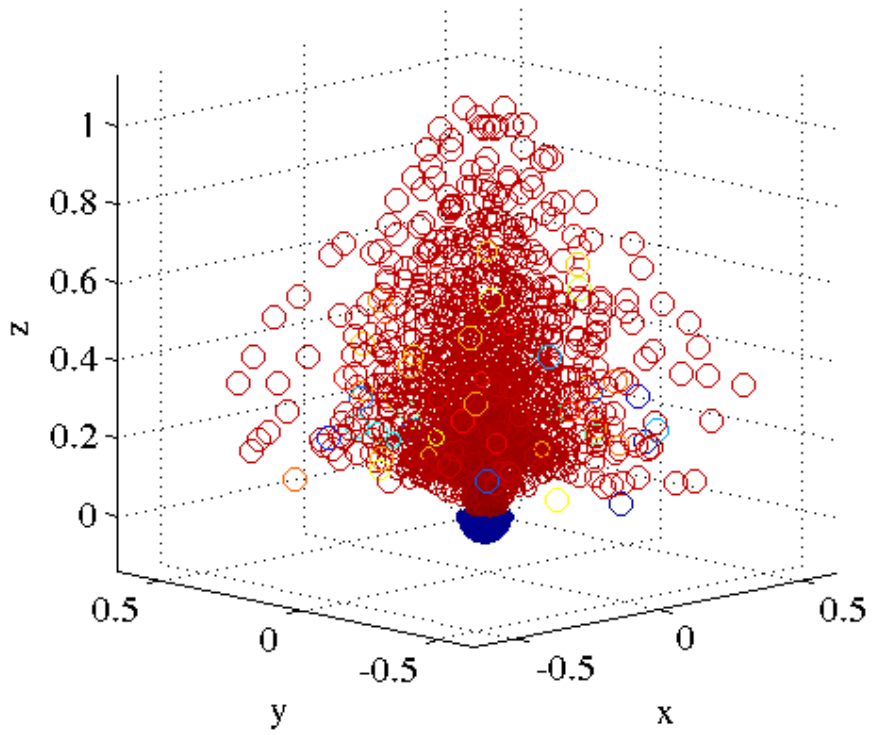

Figure 4.9 Propellant ejection from nozzle at 4.7 microseconds.

In Figures 4.7, 4.8, and 4.9, it can clearly be seen that the particles are experiencing considerably greater motion in the positive z direction compared to the x and y directions. This is consistent with the high propulsion efficiency observed.

The exact reason for why a pancake shape offers higher performance can likely be attributed to the meeting of rarefaction waves in the propellant cylinder. For a cylindrical column of gas, rarefaction waves will originate along the axial and radial surfaces and then propagate through the gas. If the gas is in the shape of a thin pancake, the rarefaction waves originating from the axial surfaces will meet much sooner than the rarefaction waves originating from the radial surfaces. The meeting of rarefaction waves from the axial surface will cause the propellant to expand axially, and the gas will then

proceed to fill much of the volume of the nozzle, allowing for better propulsion efficiency.

4.3 Pusher Plate Performance Results

Simulations of the pusher plate were run across the same parameter space as the nozzle. As with the nozzle, a thin pancake-shaped propellant mass was found to offer the best performance for the pusher plate. Figure 4.10 is provided to illustrate this geometric permutation.

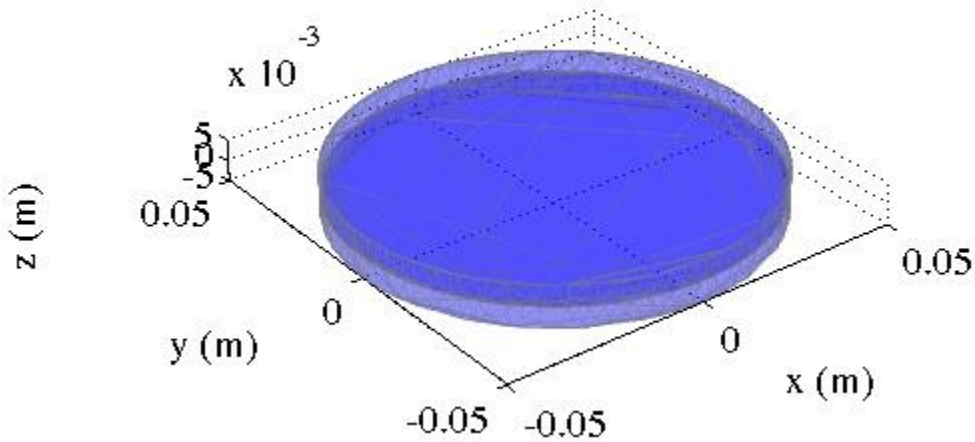

Figure 4.10 Pancake-shaped propellant against the surface of the pusher plate.

In the interests of time, the presented performance values for the pusher plate are constrained to the pancake-shaped propellant mass, with the permutations being in the temperature and number density of the propellant.

Table 4-10 Pusher plate performance with pancake-shaped propellant.

Temperature (eV)	Number Density	Specific Impulse (s)	Propulsion Efficiency
1	10^{24}	163	49.7%
1	10^{26}	170	51.6%
1	10^{28}	171	57.4%
100	10^{24}	1,691	49.6%
100	10^{26}	1,703	51.5%
100	10^{28}	1,718	57.4%
1,000	10^{24}	5,361	49.7%
1,000	10^{26}	5,381	51.6%
1,000	10^{28}	5,400	57.4%

As with the nozzle, higher specific impulse is achieved at higher propellant temperatures, as is to be expected when a greater amount of thermal energy is initially present. Variations are observed in both the specific impulse and the propulsion efficiency within the same temperature with different number density permutations, but as with the nozzle, these variations are on the order of about 5%. Again, this discrepancy may be attributable to an artifact from the numerical integration in the code.

The results from one of the pusher plate simulations will now be presented in greater detail. The initial conditions for this presented simulation are the same as those used in the detailed nozzle simulation, which consists of an initial propellant temperature of 1,000 eV and a number density of 10^{26}. Figure 4.10 and Figure 4.11 show the time evolution of the specific impulse and propulsion efficiency for the pusher plate throughout the simulation.

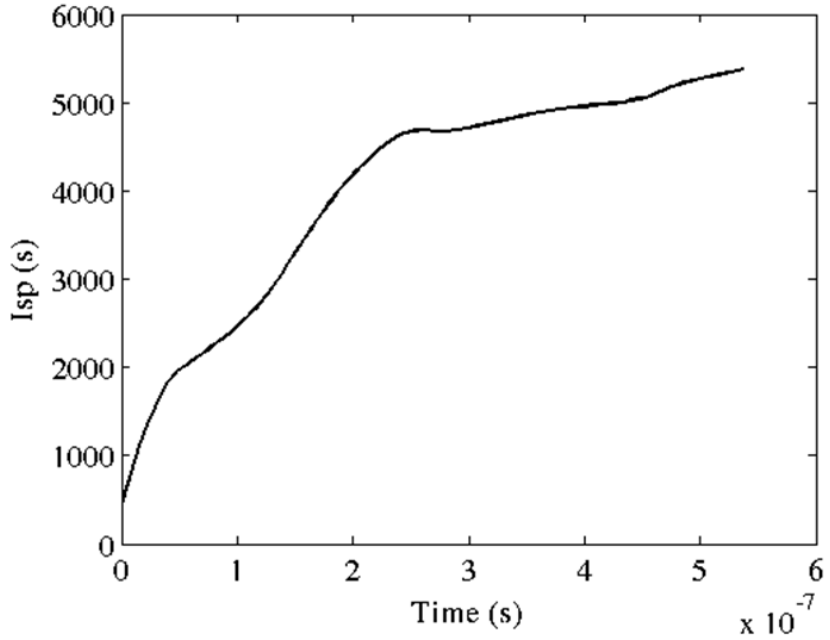

Figure 4.11 Pusher plate specific impulse.

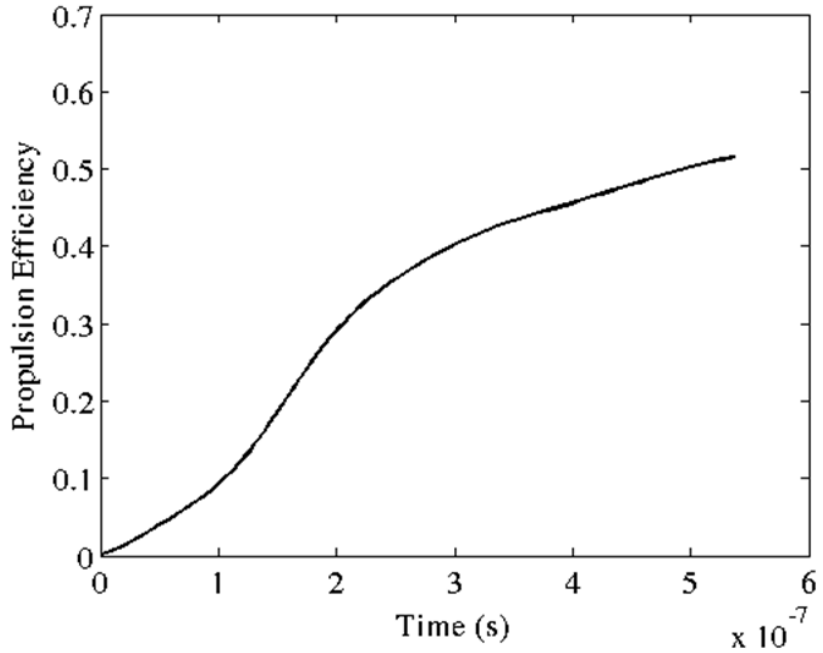

Figure 4.12 Pusher plate propulsion efficiency.

Figure 4.13 shows the propellant gas particles being ejected from the pusher plate control volume. The image is taken at a simulation time of about 0.54 microseconds, at which point more than 95% of the propellant gas particles have exited the control volume.

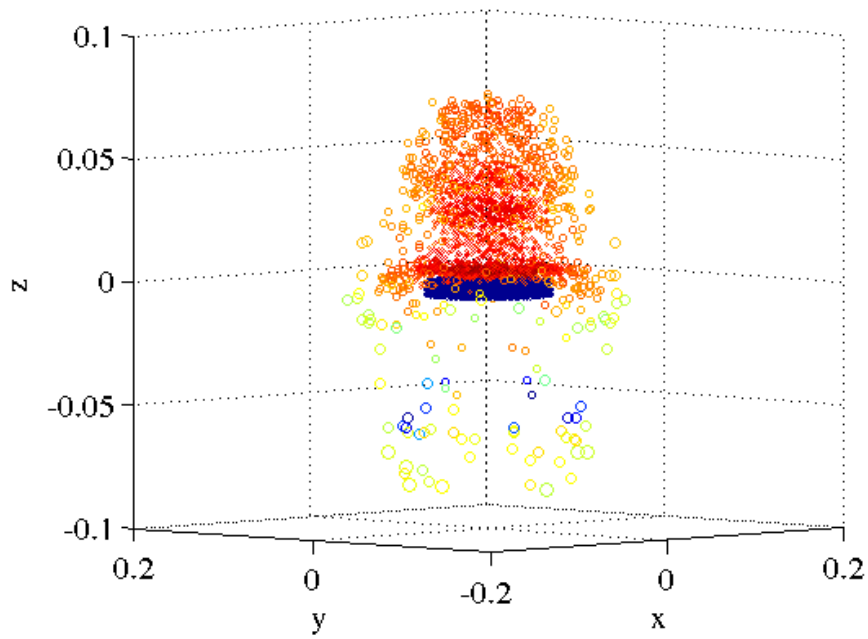

Figure 4.13 Ejection of propellant gas particles from pusher plate.

As with the nozzle, the majority of the gas particles are moving in the positive z direction away from the control volume. However, it can clearly be seen that a significant fraction of the particles are moving in the negative z direction after leaving the control volume, which was not observed at all with the nozzle.

It should also be noted that it takes nearly ten times as long for 95% of the propellant to exit the control volume of the nozzle as it takes to exit the control volume of the pusher plate. This is due to the fact that in the case of the nozzle, some of the gas

particles first move toward the far end of the nozzle until they bounce off of the nozzle wall, which then propels them outside of the control volume.

This may also help to explain why the pusher plate has considerably lower propulsion efficiency than the nozzle. In the case of the pusher plate, the particles only have a single surface to bounce off, and are able to exit the control volume of the pusher plate much sooner than particles in the nozzle. Conversely, the nozzle wall provides additional surface area for gas particles to reflect off, and this reflection converts radial and tangential momentum into axial momentum. The pusher plate lacks these walls, and so would experience a greater amount of radial and tangential momentum losses. This would explain the positions of some of the gas particles in the negative z direction as observed in Figure 4.13.

CHAPTER 5

CONCLUSIONS

This thesis explored variations in the propulsion performance of a hemispherical nozzle and a pusher based on permutations of propellant density, temperature, and geometric shape. The work was motivated by the interest in studying the ability to convert a z-pinch discharge for thermonuclear experiments into directed thrust. A parametric study was performed in 3D utilizing the new code SPFMax, which is based on the SPH numerical method.

First, the accuracy of using SPFMax in the simulation of real-world hydrodynamics problems was demonstrated. Convergence was achieved in the shock tube problem at a rate of $\sim n^{0.5}$. More than 10% accuracy was achieved in the shock tube problem with only 3,006 gas particles in three dimensions. In the simulation a gas sphere expanding into a vacuum, the average expansion velocity of the gas asymptotically approaches the maximum theoretical expansion velocity predicted by Zel'dovich and Raizer. These successful test cases provided the verification needed to use SPFMax to simulate pulsed plasma propulsion for a pusher plate and a hemispherical nozzle.

For the propulsion simulations, a cylinder of argon plasma was used as the propellant. Dimensionless scaling parameters were used to determine the general shape of a propellant cylinder to achieve high propulsion performance.

For the hemispherical nozzle, altering the shape of the propellant cylinder caused the propulsion efficiency to vary from about 36% to 72%. The 72% efficiency was obtained when the propellant was in the shape of a thin pancake with the same diameter as the nozzle.

A pancake-shaped propellant was also found to offer the highest propulsion efficiency for a pusher plate. However, the efficiency was substantially less than that of the nozzle, on the order of about 50%. This can be attributed to the nozzle walls providing more surface area for the gas particles to rebound from, which helps to convert radial and tangential momentum into axial momentum.

These findings help provide guidance for future research in this field. For example, future studies may focus on the feasibility of a making a propellant gas assume the shape of a pancake when it first begins to expand within a nozzle. If this shape proves to be too difficult to create, then alternate propellant shapes should be investigated that are able to balance performance with practicality.

The successful utilization of SPFMax for the work in this thesis opens the door for many future studies that may benefit from utilizing this code. This includes advanced propulsion concepts and high energy equations of state, fields in which there are many topics deserving of continued research. The hope is to eventually include the effects of electromagnetics in SPFMax simulations. This could allow SPFMax to simulate the interactions of fluid flows with circuit models, a useful capability in the study of other advanced propulsion systems such as magnetic nozzles.

The simulation of magnetic nozzles is an area of research that should be investigated for advanced pulsed propulsion. Future studies may focus on comparing the

performance of the hemispherical nozzle to magnetic nozzles. The main advantage that solid state nozzles have over magnetic nozzles is the simplicity, and it should also be noted that the efficiency of solid-state nozzles was found to be on the order of 72% in this thesis. This efficiency is on the same order of what other studies have reported for magnetic nozzles. Using magnetic nozzles would also require large capacitor banks that would add to both the power and mass requirements. As such, any higher efficiency levels that may be offered by magnetic nozzles must be carefully weighed against the additional mass and complexity associated with such a system.

Ablation of nozzle materials is a major concern that should also be addressed in future studies. One possible solution to this is to apply oil to the surface of the nozzle. The researchers for Project Orion found that applying oil to the surface of the pusher plate was very effective in reducing ablation. New materials that were not available in the 1950s and 1960s may further help to mitigate ablation.

Ultimately, the hope is that the work in this thesis will help lay the foundation for future pulsed fusion propulsion experiments that may be done at the University of Alabama in Huntsville. These experiments may focus on creating plasmas that could be utilized on fusion propelled spacecraft, and deriving propulsive thrust using a mechanism such as a hemispherical nozzle is of great significance to these future experiments.

No major technological barriers exist that prevent pulsed nuclear propulsion from being utilized now. The absence of spacecraft utilizing such propulsion systems can be attributed primarily to political and social opposition. Project Orion was an unfortunate casualty of efforts to mitigate the nuclear arms race between the United States and Soviet Union. Further anti-nuclear sentiments grew as a result from fear of nuclear weapons

proliferation and disasters that occurred at Chernobyl, Three Mile Island, and Fukushima. This resistance has imposed constraints on nuclear propulsion research, and it is unlikely that this opposition will subside in the foreseeable future. These constraints must be acknowledged and incorporated into the planning of any future studies involving pulsed nuclear propulsion in order for such projects to have any chance of success.

REFERENCES

[1] G. Sutton and O. Biblarz, Rocket Propulsion Elements, Eighth Edition, New York, NY: John Wiley& Sons Inc. , 2010.

[2] R. Frisbee, *Journal of Propulsion and Power*, vol. 19, no. 1129, 2003.

[3] A. Charania, B. S. Germain, J. Wallace and J. Olds, "REACTIONN: A Nuclear Electric Propulsion Mission Concept to the Outer Solar System," in *40th AIAA/ASME/SAE/ASEE Joint Propulsion Conference and Exhibit*, Fort Lauderdale, FL, 2004.

[4] M. Clausery, Proceedings of the Conference on Extremely High Temperatures, John Wiley and Sonce, Inc., 1958.

[5] S. Maslen, *Military Electronics, IRE Transactions On MIL-3, 52,* vol. 52, 1959.

[6] J. Cassibry, R. Cortez, M. Stanic, W. Seidler, R. Adams, G. Statham and L. Fabisinki, "The Case and Development Path for Fusion Propulsion".

[7] "Space Station Mission Expedition 30-31," National Aeronautics and Space Administration, November 2011.

[8] W. Moeckel, "Propulsion Systems for Manned Exploration of the Solar System," NASATM-X-1864, 1969.

[9] W. Moeckel, *Journal of Spacecraft and Rockets*, vol. 9, no. 12, p. 863, 1972.

[10] B. Wagstaff, "A Spaceship Named Orion," Air & Space, Smithsonian Institute, 1988.

[11] "Nuclear Pulse Space Vehicle Study," George C. Marshall Space Flight Center,

Huntsville, AL, 1964.

[12] G. Dyson, "Project Orion: The True Story of the Atomic Spaceship," Henry Holt and Co., New York, NY, 2002.

[13] J. D. Balcomb, L. Booth, T. Cotter, J. Hedstrom, C. Robinson, T. Springer and C. Watson, "Nuclear Pulsed Space Propulsion Systems," LA-4541-MS, Los Alamos Scientific Laboratory, Los Alamos, NM, November 1970.

[14] J. C. Solem, "Medusa: Nuclear explosive propulsion for interplanetary travel," *Journal of the British Interplanetary Society,* vol. 46, no. 1, p. 21–26, 1993.

[15] J. C. Solem, "Nuclear explosive propulsion for interplanetary travel: Extension of the MEDUSA concept for higher specific impulse," *Journal of the British Interplanetary Society,* vol. 47, no. 6, p. 229–238, 1994.

[16] R. Hyde, L. Wood and J. Nuckolls, "Prospects for rocket propulsion with laser-induced fusion microexplosions," AIAA Paper No. 72-1063, December 1972.

[17] R. A. Hyde, "A Laser Fusion Rocket for Interplanetary Propulsion," in *34th International Astronautical Federation*, Budapest, Hungary, 10-17 October 1983.

[18] F. Winterberg, "Rocket propulsion by thermonuclear micro-bombs ignited with intense relativistic electron beams," *Raumfahrtforschung,* vol. 15, pp. 208-217, 1971.

[19] A. Bond, A. Martin and et al., "Project Daedalus – The Final Report on the BIS Starship Study," *Journal of British Interplanetary Society*, 1978.

[20] K. Beals, M. Beaulieu, F. J. Dembia, J. Kerstiens, D. L. Kramer, J. R. West and J. A. Zito, "Project Longshot: An Unmanned Probe To Alpha Centauri," U S Naval

Academy. NASA-CR-184718, 1988.

[21] K. Long, R. Obousy and A. Hein, "Project Icarus: Optimisation of nuclear fusion propulsion for interstellar missions," *Acta Astronautica*, vol. 68, pp. 1820-1829, 2011.

[22] R. K. Obousy, "Vacuum to Antimatter-Rocket Interstellar Explorer System (VARIES): A Proposed Program for an Interstellar Rendezvous and Return Architecture," *Journal of the British Interplanetary Society*, vol. 64, pp. 378-386, 2011.

[23] M. Stanic, J. Cassibry and R. Adams, "Project Icarus: Analysis of Plasma jet driven Magneto-Inertial Fusion as potential primary propulsion driver for the Icarus probe," *Acta Astronautica*, vol. 86, pp. 47-54, 2013.

[24] C. Orth, "VISTA - A Vehicle for Interplanetary Space Transport Application Powered by Inertial Confinement Fusion.3," Lawrence Livermore National Laboratories: Livermore, California, 2003.

[25] Y. Thio, B. Freeze, R. Kirkpatrick, B. Landrum, H. Gerrish and G. Schmidt, "High-Energy Space Propulsion based on Magnetized Target Fusion," in *35th AIAA/ASME/SAE/ASEE Joint Propulsion Conference and Exhibit*, Los Angeles, California, 1999.

[26] R. Adams, R. Alexander, J. Chapman, S. Fincher, R. Hopkins, A. Philips, T. Polsgrove, R. Litchford, B. Patton, G. Statham, P. White and Y. Thio, "Conceptual Design of In-Space Vehicles for Human Exploration of the Outer Planets," 2003.

[27] A. K. Martin, R. H. Eskridge, P. J. Fimognari and M. H. Lee, "FIREBALL: Fusion

Ignition Rocket Engine with Ballistic Ablative Lithium Liner," *AIP Conference Proceedings*, vol. 813, no. 1, pp. 783-794, 2006.

[28] Maslen, "Results for Icarus optimistic scenario with S.H.," *IRE Transactions on Military Electronics*, vol. 3, no. 52, 1959.

[29] F. H. Ebersohn, S. S. Girimaji, D. Staack, J. V. Shebalin, B. Longmier and C. Olsen, "Magnetic Nozzle Plasma Plume: Review of Crucial Physical Phenomena," in *48th AIAA /ASME/SAE/ASEE Joint Propulsion Conference & Exhibit*, Atlanta, GA, 2012.

[30] E. Ahedo and M. Merino, "Two-dimensional plasma expansion in a magnetic nozzle: Separation due to electron inertia," *Physics of Plasmas*, vol. 19, 2012.

[31] R. Hoyt, "Magnetic Nozzle Design for High-Power MPD Thrusters," in *29th International Electric Propulsion Conference*, Princeton University, 2005.

[32] A. Arefiev and B.N. Breizman, "Theoretical Components of the VASIMR plasma propulsion concept," *Physics of Plasmas*, vol. 11, no. 5, pp. 2942-29-49, 2004.

[33] F. Diaz, "An overview of the VASIMR engine: High power space propulsion with RF plasma generation and heating," in *AIP Conference*, 2001.

[34] A. Ilin, "Simulations of Plasma Detachment in VASIMR," in *40th AIAA Aerospace Sciences Meeting and Exhibit*, Reno, Nevada, 2002.

[35] Ad Astra Rocket Company, [Online]. Available: http://www.adastrarocket.com/aarc/Technology. [Accessed 4 May 2013].

[36] I. Mikellides, P. G. Mikellides, P. J. Turchi and T. M. York, "Design of a Fusion Propulsion System- Part 2: Numerical Simulation of Magnetic-Nozzle Flows," *Journal of Propulsion and Power*, vol. 18, no. 1, pp. 152-158, 2002.

[37] I. Mikellides, P. G. Mikellides, P. J. Turchi and T. M. York, "Numerical simulation of magnetically-guided plasma flows for the design of a fusion propulsion system," *AIP Conference Proceedings,* vol. 552, no. 1, pp. 900-907, 2001.

[38] J. Gilland, C. Williams, I. Mikellides, P. Mikellides and D. Marriott, "Multi-Megawatt MPD Plasma Source Operation and Modeling for Fusion Propulsion Simulations," in *AIP Conference*, 2004.

[39] C. Sijoy and C. Shashank, "Conversion of plasma into electrical pulse by magnetic flux compression," *Fusion Engineering and Design,* vol. 86, pp. 174-182, 2011.

[40] Y. Nagamine and H. Nakashima, "Analysis of plasma behavior in a magnetic thrust chamber of a laser fusion rocket," *Fusion Technology,* vol. 35, p. 62–70, 1999.

[41] N. Sakaguchi, Y. Kajimura and H. Nakashima, "Thrust Efficiency Calculation for Magnetic Nozzle in Laser Fusion Rocket," *Transactions of the Japan Society for Aeronautical and Space Sciences,* vol. 48, no. 161, pp. 180-182, 2005.

[42] Y. Kajimura, R. Kawabuchi and H. Nakashima, "Control techniques of thrust vector for magnetic nozzle in laser fusion rocket," *Fusion Engineering and Design,* vol. 81, no. 23, pp. 2871-2875, 2006.

[43] N. Matsuda, A. Maeno, Y. Kajimura and H. Nakashima, "A magnetic nozzle chamber design for a laser fusion rocket based on impact fast ignition," in *14th International Congress on Plasma Physics*, Fukuoka, Japan, 2008.

[44] A. Maeno, T. Hanaya, N. Yamamotoz, H. Nakashima, S. Fujioka, A. Sunahara and T. Johza, "Preliminary Experiments for Demonstrating Magnetic Thrust Chamber Concept in Laser Fusion Rocket," in *31st International Electric Propulsion*

Conference, Ann Arbor, Michigan.

[45] P.-O. Persson and G. Strang, "A Simple Mesh Generator in MATLAB," *SIAM Review*, vol. 46, no. 2, pp. 329-345, 2004.

[46] P.-O. Persson, *Mesh Generation for Implicit Geometries*, Cambridge, MA: PhD Thesis, Department of Mathematics, MIT, 2004.

[47] G. Alaa, E. Francomanob, A. Tortoricib, E. Toscanob and F. Violaa, "Smoothed Particle ElectroMagnetics: A mesh-free solver for transients," *Journal of Computational and Applied Mathematics*, vol. 191, pp. 194-205, 2006.

[48] B. C. Low, "Self-Similar Magnetohydrodynamics. IV. The Physics of Coronal Transients," *The Astrophysics Journal*, vol. 281, pp. 392-412, 1984.

[49] R. Gingold and J. Monaghan, "Smoothed particle hydrodynamics: theory and application to non-spherical stars," *Monthly Notices of the Royal Astronomical Society*, vol. 181, pp. 375-389, 1977.

[50] L. Lucy, "A numerical approach to the testing of the fission hypothesis," *The Astronomical Journal*, vol. 82, pp. 1013-1024, 1977.

[51] J. Monaghan, "Smoothed particle hydrodynamics," *Reports on Progress in Physics*, vol. 68, pp. 1703-1759, 2005.

[52] G. Liu and M. Liu, Smoothed Particle Hydrodynamics: A Meshfree Particle Method, 2003.

[53] J. Anderson, "Chapter 7 Unsteady Wave Motion," in *Modern Compressible Flow: With Historical Perspective*, McGraw-Hill Science Engineering, 2002.

[54] L. D. G. Sigalotti, H. Lopez, A. Donoso, E. Sira and J. Klapp, "A shock-capturing

SPH scheme based on adaptive," *Journal of Computational Physics*, vol. 212, p. 124–149, 2006.

[55] J. M. Stone, J. F. Hawley, C. R. Evans and M. L. Norman, "A Test Suite for Magnetohydrodynamical Simulations," *The Astrophysical Journal*, vol. 388, pp. 415-437, 1992.

[56] Y. B. Zel'dovich and Y. P. Raizer, in *Physics of Shock Waves and High-Temperature Hydrodynamic Phenomena*, Mineola, NY, Dover Publications, 2002, p. 103.